

KUNGLIGA TEKNISKA HÖGSKOLAN
PHELMA

Master in Energy and Nuclear Engineering
Reactor Physics Department

Master Thesis



Ab Initio based Multi-Scale
Simulations of Oxide Dispersion
Strengthened Steels

Antoine Claisse

Supervisors:

Dr. Pär Olsson

Dr. David Rodney

Academic year 2011-2012

*“All you create, all you destroy,
All that you do, all that you say [...]
And everything under the sun is in tune
But the sun is eclipsed by the moon.*

Pink Floyd, 1973

Abstract

The growing need to produce clean energy requires the development of new nuclear plants using less fissile materials. These plants operate at high temperatures and yield high neutron fluxes. The current structural materials can not withstand these conditions and a new class of steels is therefore under development. These steels must be resistant to swelling, ductile to brittle transition temperature shift and creep induced by irradiation. The Oxide Dispersion Strengthened (ODS) steels seem to be a good answer to these requirements and the experiments confirm that their mechanical properties are much better than for classic austenitic and ferritic-martensitic steels. However, their performances are due to the high density of oxide nanoclusters in the material, which trap helium before it forms bubbles and prevent the dislocations from moving, and these clusters are not well understood yet.

An ab-initio study has been performed on Cr, Y, Ti and O in an iron lattice using the Density Functional Theory (DFT). The stable position of each of these solutes in the iron matrix has firstly been determined. Then, all the pair interactions of the solutes between each other and with a vacancy have been calculated up to the fifth nearest neighbour, as well as the migration energy of these solutes. The goal of these simulations was to obtain enough data to understand the formation process of (Y,Ti,O) clusters in an iron lattice. Special considerations have been given to the interactions between a vacancy and an yttrium atom and a vacancy and oxygen atoms, in both cases because of the very strong attraction between them. The second part of this work is based on Atomistic Kinetic Monte Carlo (AKMC) simulations of systems using the data acquired from the first-principles calculations. Due to calculating power constraints, several approximations had to be done for the migration energies of Y and O. This caused a difficulty in converting the AKMC code time into a real time. Additional simulations were run to try to establish the stability range of the clusters. The results show that (Y,Ti,O) clusters can be formed at 1200 K thanks to the vacancy assisted diffusion mechanism. They are reasonably stable at 600 K without vacancy, but a vacancy helps achieving a higher stability. A vacancy can also trap up to 6 oxygens.

Sammanfattning

Det växande behovet att producera ren energi kräver utvecklingen av nya kärnkraftverk som använder mindre klyvbara ämnen. Dessa verkar vid höga temperaturer och skapar höga neutronflöden. De nuvarande strukturella materialen tål inte dessa villkor och en ny klass av stål är därför under utveckling. Dessa stål måste tåla svullnad, omslagstemperaturförskjutning och kryppning, alla av dessa under bestrålning. Oxidförstärkta stål (ODS) ser ut som ett bra svar för dessa behov och erfarenheter bekräftar att deras mekaniska egenskaper är mycket bättre än för de traditionella austenistiska och ferritisk-martensistiska stålen. Deras prestationförmåga beror på den höga densiteten av oxidkluster i materialet som fångar helium innan de skapar bubblor, och förhindrar dislokationernas förflyttning, och dessa kluster ä inte än förstådda.

En ab initio analys genomfördes med Cr, Y, Ti och O i en järnmatris med hjälp av täthetsfunktionalteorin (DFT). Varje elements stabila position i järnmatrisen uträndes först. Därefter beräknades alla parväxelverkan mellan dessa atomer och mellan dem och en vakans upp till den femte närmaste grannen. Migrationenergin beräknades också. Målet med dessa simuleringar är att skaffa tillräckligt med data för att förstå formationprocessen av (Y,Ti,O) kluster i en järnmatris. Särskild hänsyn gavs till växelverkan mellan en vakans och en yttriumatom och mellan en vakans och syreatomer, eftersom det finns en mycket stark växelverkan mellan dem två i båda fallen. Den andra delen av detta arbete grundas på atomistisk kinetisk Monte Carlo (AKMC) simulationer som använder ab initio data från den första delen. På grund av beräkningskraftbegränsningar gjordes några approximationer på migrationenergin av Y och O. Detta medförde en svårighet för att konvertera AKMC tiden till verklig tid. Fler simulationer utfördes för att försöka att etablera stabilitetsområdet för dessa kluster. Resultatet är att (Y,Ti,O) kluster kan skapas vid 1200 K tack vare den vakansdrivna diffusionmekanismen. De är rimligt stabila vid 600 K utan vakanser, men en vakans hjälper att nå en högre stabilitet. En vakans kan också fånga upp till sex syreatomer.

Résumé

La demande croissante en énergie propre exige le développement de nouvelles centrales nucléaires utilisant moins de matériaux fissiles. Ces centrales fonctionnent à température élevée et produisent d'importants flux de neutrons. Les matériaux de structure actuels ne sont pas capables de supporter ces conditions, et un nouveau type d'aciers est donc en développement. Ces aciers doivent être résistants au gonflement, au décalage de la température de transition ductile-fragile et au fluage, le tout sous irradiation. Les aciers durcis par dispersion d'oxydes (ODS) semblent bien répondre à ces demandes et les expériences confirment que leurs propriétés mécaniques sont bien meilleures que celles des aciers classiques tels que les austénitiques et les ferritiques-martensitiques. Cependant, leurs performances sont dues à la haute densité de nano-amas d'oxydes dans le matériau qui piègent les atomes d'hélium avant qu'ils ne puissent former des bulles et empêchent les dislocations de bouger. Ces amas ne sont pas encore bien compris.

Une étude *ab initio* sur le chrome, l'yttrium, le titane et l'oxygène dans un cristal de fer a été effectuée en utilisant la théorie de la fonctionnelle de la densité (DFT). La position d'équilibre de ces atomes en solution solide dans un cristal de fer a été déterminée dans un premier temps. Ensuite, toutes les interactions de paire entre ces atomes et entre ces atomes et une lacune ont été calculées jusqu'au 5^{ème} plus proche voisin. Les énergies de migration de ces éléments ont également été calculées. Le but de ces simulations était d'obtenir des informations sur le processus de formation des amas de (Y,Ti,O) dans un cristal de fer. Une attention particulière a été apportée aux interactions entre une lacune et un atome d'yttrium et entre une lacune et des atomes d'oxygène, dans les deux cas à cause de l'attraction très forte entre eux. La seconde partie de ce travail est basée sur des simulations Monte Carlo cinétiques atomistiques (AKMC) de systèmes en utilisant les données issues des simulations *ab initio*. A cause de limitations sur la puissance de calcul disponible, plusieurs approximations ont dû être faites concernant les énergies de migration de Y et O. Cela a causé des difficultés dans la conversion du temps Monte Carlo en temps réel. Des simulations additionnelles ont été faites pour essayer de trouver le domaine de stabilité des amas. Les résultats montrent que les amas de (Y,Ti,O) peuvent être formés à 1200 K grâce au mécanisme de diffusion assistée par lacune. Ils sont raisonnablement stables à 600 K sans lacune, mais une lacune aide à atteindre une plus grande stabilité. Une lacune peut aussi piéger jusqu'à 6 atomes d'oxygène.

Acknowledgements

I wish to use this page to thank many people, some of them I never had the occasion to do it *viva voce*. A lot of people have helped me becoming who I am today, both on a professional and on a personal level, and I start with a general thank you.

Three years ago, I found myself hesitating between different fields of physics. I was not able to make a decision, and therefore was multiplying the introductory classes. That is when I met Roger Brissot. His passion about nuclear science was remarkable. He has this unique ability to make the students want to know more all the time. He is the reason I chose nuclear sciences over other exciting topics. Three years after, I am really enjoying what I am doing, so to him, I address a special thank.

Another teacher who inspired me more than he thinks is David Rodney. He taught me my first notions of numerical analysis and gave me the opportunity to work one summer with one of his former co-worker in the research field. We had a really inspiring talk about research and especially simulations and, if I remember turning him down when he offered me a PhD, I am now convinced that this is what I want to do. I hope to have the occasion to work with you one day, and I am already grateful for all you did for me.

I enjoyed very much doing my master thesis at KTH, in the Reaktorfysik department. Everyone there was friendly with me, and helped me when I needed help. I'd like to thank Pär Olsson, for his help, his patience and his availability. He has many times given me advices and always answered my questions with a great precision and kindness. He trusted me to carry on this research and pushed me to give the best at all time. I have learnt a lot from him and am really thankful.

I also wish to thank my friends and my family, who have always been there for me. Thank you Fabio, Milan, Sarah, Zhonweng and everyone who contributed to make the working environment and the lunchtimes so pleasant. Many thanks to my Erasmus friends; Clara, Tobias, Victor, Nacho and of course Sibel, for dinners, apple cakes, sport, games, and about everything not work-related for the last 18 months. Merci maman et papa for always supporting me in my choices and thank you Justine for proving me that friendship is stronger than distance, and of course the careful proofreading of this thesis.

I acknowledge financial support from the European Fusion Development Agreement (EFDA). Most of the computer simulations have been performed on the resources provided by the Swedish National Infrastructure for Computing (SNIC) at PDC.

Abbreviations and nomenclature

0.0.0.1 List of abbreviations

1-5NN	- First-Fifth Nearest Neighbour
ACRDF	- Averaged Compared Radial Distribution Function
AKMC	- Atomistic Kinetic Monte Carlo
BCC	- Body-centered cubic (cell)
DBTT	- Ductile-brittle transition temperature
dpa	- Displacements per atom
DFT	- Density Functional Theory
FCC	- Face-centered cubic (cell)
FIA	- Foreign Interstitial Atom
Gen-IV	- Generation IV
HEG	- Homogeneous Electron Gas
HF	- Hartree-Fock
HK	- Hohenberg Kohn
GGA	- Generalized Gradient Approximation
KTH	- Kungliga Tekniska Högskolan
LAKIMOCA	- LAttice KInetic MOnTe CARlo
LDA	- Local Density Approximation
MC	- Monte Carlo
MD	- Molecular Dynamic
MEP	- Minimum Energy Path
NEB	- Nudged Elastic Band
ODS	- Oxide Dispersion Strengthened
PAW	- Projector Augmented Wave
PBE	- Perdew Burke Ernzerhof
SIA	- Self Interstitial Atom
VASP	- Vienna Ab-initio Simulation Package

0.0.0.2 Element symbols

C	- Carbon
Cr	- Copper
Fe	- Iron
He	- Helium
Mo	- Molybdenum
Mn	- Manganese
Nb	- Niobium
Ni	- Nickel
O	- Oxygen
P	- Phosphorus
S	- Sulfur
Si	- Silicon
Ti	- Titanium
V	- Vacancy (not Vanadium in this work)
W	- Tungsten
Y	- Yttrium
Zr	- Zirconium

0.0.0.3 Physical quantities

k_B	- Boltzmann's constant
-------	------------------------

Contents

Abstract	V
Sammanfattning	VI
Résumé	VII
Acknowledgements	VIII
Nomenclature	IX
List of Figures	XIII
List of Tables	XIV
1 Introduction/Motivations	1
1.1 Background	1
1.2 Aims of the work	3
2 Theoretical background	5
2.1 Density Functional Theory	5
2.1.1 Hamiltonian	6
2.1.2 Wavefunctions	11
2.1.3 Vienna Ab-initio Simulation Package	14
2.2 Kinetic Monte Carlo	15
2.2.1 Atomic Kinetic Monte Carlo	18
2.2.2 LAttice KInetic MOnte CARlo	19
2.3 Materials irradiation	20
2.3.1 Defects	20
2.3.2 Energies	21
2.3.3 Macroscopic effect of irradiation	22
2.3.4 Oxide Dispersion Strengthened (ODS) steels	25

3	Results	27
3.1	Ab-initio calculations	27
3.1.1	stable position of solutes	28
3.1.2	Interactions with vacancies	31
3.1.3	Migration of the solutes	37
3.1.4	Interactions between solutes	40
3.1.5	Clustering	43
3.2	Atomic kinetic Monte-Carlo	46
3.2.1	Approximations and modifications	46
3.2.2	Formation of clusters	49
3.2.3	Stability of clusters under normal conditions	55
4	Conclusions	57

List of Figures

2.1	Flow-chart of a typical DFT calculation within the Kohn-Sham framework.	9
2.2	Illustration of the pseudopotential and of the pseudo wave-function.	12
2.3	Illustration of the images in the NEB method	16
2.4	Map of the simulation methods depending on the aimed timescale and lengthscale.	17
2.5	Different types of defects in a crystal	20
2.6	Influence of the chromium content on the DBTT shift.	24
3.1	Tensile, compressed and mixed sites.	28
3.2	5 nearest octahedral position from a regular lattice site	32
3.3	Illustration of a couple V-O moving.	34
3.4	Geometry of vacancy-oxygen clusters.	35
3.5	Relaxation of the oxygen atoms around a vacancy.	36
3.6	Differential electron density for 1 and 6 octahedral O around a vacancy.	37
3.7	Illustration of the Y-V relaxation.	39
3.8	Position of the Y atom when first nearest neighbour of a vacancy for a temperature oscillating around 2000 K.	39
3.9	Illustration of the vacancy diffusion mechanism.	40
3.10	The eleventh nearest octahedral neighbours of an octahedral site.	43
3.11	Binding energy of O with it's eleventh first nearest neighbours O.	44
3.12	Most stable configurations for Y_2TiO_3	45
3.13	System Cr-Ti at 1200 K after 2.9 seconds.	51
3.14	System Cr-Y at 1200 K after 98 days.	51
3.15	System Cr-Ti-Y at 1200 K after 90 days.	52
3.16	System Cr-Ti-O at 1200 K after 37 μ s.	53

3.17 System Cr-Y-O at 1200 K after 127 μs	53
3.18 System Cr-Ti-Y-O at 1200 K after 153 μs	54
3.19 Clusters at 1200 K after 153 μs	54

List of Tables

2.1	Value of π given by a MC process depending on the number of events	17
2.2	Composition of some steels in weight %.	23
3.1	Solution energies (eV)	30
3.2	Binding energies (eV) SIA-solute	31
3.3	Distance between the nearest neighbours (in unit of lattice parameter	31
3.4	Binding energies with a vacancy.	33
3.5	Binding and relative binding energies of oxygens with a vacancy.	36
3.6	Migration energies of solutes in an iron BCC lattice.	37
3.7	Binding energies of solutes with Cr.	41
3.8	Binding energies of solutes with Ti.	42
3.9	Binding energies of solutes with Y.	42
3.10	Value of the time conversion coefficient.	50

Chapter 1

Introduction/Motivations

1.1 Background

In the global effort to reduce the emissions of greenhouse gases, the coal and gas plants have to be limited in favor of clean energies, such as renewable and nuclear energies. However, the uranium reserves are limited and current reactors will run out of fuel in the next decades or centuries. It is then necessary to develop new technologies to overcome this issue; the fourth generation of breeder reactors or, in a hypothetical future, the fusion reactors will drastically reduce the need for rare materials for the fuel. In addition to that, they will produce much less nuclear wastes, and the fission reactors can even burn some with an appropriate design. These new technologies operate at high temperatures, in non chemically inert environments and produce high neutron radiation fields. These peculiar conditions, and especially the irradiation, lead to a need in a new class of materials able to withstand such an environment. For the structural materials usually made of steels, this means that they need to be made more radiation resistant. A tremendous effort is made in investigating several kinds of steels with different phases for the iron lattice as well as different compositions, in order to find those which are most likely to be a solution.

Previous studies have already shown that the three main issues with structural steels are swelling, embrittlement, and thermal creep. These problems can weaken the answer to transient and lower the resistance to fatigue. Concerning swelling, austenitic steels (with a face-centered cubic (fcc) structure) can in the best case resist 120 displacements per atom on average (dpa), due to the production of helium. This case is reached if titanium is present in the steel. However, to keep the crystal structure, nickel is present to act as a stabilizer and has a high (n,α) cross section. Ferritic-martensitic

steels (with a body-centered cubic (bcc) structure), without nickel, can resist around 200 dpa, which would correspond to around five years in a fast neutrons reactor. The ductile to brittle transition temperature shift is mainly a problem at low temperature, when irradiation yields a larger shift. The shift can reach up to 250 degrees depending on the conditions and is lower in presence of chromium. The thermal creep is mostly an issue for irradiation at high temperature and for this problem as well as for the embrittlement, austenitic steels are better than the ferritic-martensitic ones.

However, as good as these steels are, they all have drawbacks and it is necessary to develop a new technology which would have both a high creep strength, to allow operating at higher temperatures than the displacement damage regime limit, and be resistant to swelling, trapping the He atoms before they do any damage, forming bubbles. One of the most promising way to fulfill these requirements is to use oxide dispersion strengthened (ODS) steels. These steels have usually a bcc iron lattice with different solutes such as chromium, titanium, and tungsten. Yttrium and oxygen can be mechanically alloyed by ball milling. This is followed by a heat treatment during which oxide clusters are formed. It has been noticed that the Y-Ti-O clusters give good experimental results. They can appear in a near stoichiometric composition, such as $Y_2Ti_2O_7$ or Y_2TiO_5 or in the simpler oxide form Y_2TiO_3 . It is reasonable to think that the smallest of these clusters is the base for the other ones and should therefore be studied.

Nevertheless, the dynamic of these nanoclusters formation is not well established yet, neither is their behaviour under irradiation. In addition to the experimental work proving that Y_2O_3 clusters don't exist[1], that titanium reduces the size of the clusters and confirming the existence of $Y_2Ti_2O_7$ or Y_2TiO_5 [2][3], it is important to have a model that can provide an answer to the observed behaviours. Thanks to ab-initio studies, data of the cohesive energies of the self interstitial atoms (SIA) [4][5][6], of the solution energy of oxygen, yttrium and titanium [6][7] and their binding energies with a vacancy [7] have been provided. Jiang et. Al. have also calculated the binding energy between Y, Ti and O in interstitial and substitutional positions up to the second nearest neighbour. When C.L. Fu stated that the formation of oxide nanoclusters is impossible without the help of vacancies [8], Jiang et. Al. have shown that Y_2TiO_3 clusters can be in theory formed in a vacancy-free lattice. Also using density functional theory and nudged elastic band method, Murali and coworkers have calculated the diffusion coefficients of Fe, Y, Ti and Zr by the vacancy mechanism using the nine frequencies model of Le Claire [9][10]. Hin and Wirth have shown that Y_2O_3 and Ti_2O_3 clusters are form in bcc iron lattice using a Monte Carlo method

[11][12].

Notwithstanding this previous work, a full simulation is still missing. This simulation should include the above mentioned elements as well as chromium, and should use results from first principles methods to build up a kinetic monte carlo model from which the formation mechanisms and the answer of the cluster when one of its atom is knocked out due to irradiation could be observed. Indeed, Cr is present in all the steels to reduce the swelling and the DBTT shift. These previous studies also focused on the very short range interactions, typically up to the second neighbour. If the long range interactions will obviously be negligible, it is still useful to consider them up to the fifth nearest neighbour. Concerning the kinetic of these systems, the formation of clusters including Y, Ti and O hasn't been considered, and the work on Y_2O_3 and Ti_2O_3 uses experimental values and not first principles ones. This thesis is based on these observations.

1.2 Aims of the work

The aim of this thesis work is to find out the behaviour of the clusters in ODS steels. The considered oxides are (Y,Ti,O). Three stages of the oxides life are of peculiar interest: the formation, the stability under normal conditions, and the stability under irradiation.

In order to achieve that goal, the interactions between each component of the steel have to be found. Analysing the cohesive energies of Cr, Ti, Y and O in different positions in a bcc iron matrix enables to deduce the most stable one. From these positions, binding energies up to the fifth nearest neighbour (distance at which the interaction becomes weak enough to be neglected) have to be computed. They will give information about the composition and the geometric configuration of the clusters. The migration energies of a substitutional atom by the vacancy diffusion mechanism and of interstitial atoms must also be calculated to be able to simulate the kinetics of the system. All these data will be found using the Vienna Ab-initio Simulation Package (VASP). Results are displayed and commented in Chapter 3.

Using these data in a lattice kinetic Monte Carlo code (LAKIMOCA) will provide the evolution of an iron lattice with defects after metal alloying. The idea is to run simulations covering a broad spectrum of initial compositions to determine the influence of each component. Then, seeing the formation of clusters would be a validation of the entire work, whereas not seeing it would mean that a better model has to be found. Still using LAKIMOCA, and starting from a configuration with clusters, the stability of these clusters, will be studied during reactor lifespan timescales.

Chapter 2

Theoretical background

A basic theoretical knowledge will be provided through this chapter. To understand the physics of point defects, and in this thesis, applied to nanocluster formation and the response to irradiation, it is necessary to have a closer look at the materials, at an atomic scale. The theory at this scale is quantum mechanics, and it should be possible to predict everything derived from the energy solving the Schrödinger equation. However, it is impossible with today computers to solve it for systems of more than a few electrons. The problem doesn't lie with computers power, but with the exponential increase of the number of parameters required to solve this equation [13]. Another approach is hence needed: This is where the Density Functional Theory (DFT) comes. The underlying framework will be described in this part. The knowledge in materials science that is needed to understand the point defect simulations and the influence of these defects on macroscopic and microscopic properties will also be provided. It will also be explained how an oxide dispersion strengthened (ODS) steel can overcome some of the encountered issues, discussed in introduction and in section 2.3.3.

In this chapter, Hartree atomic units are used for convenience, that is to say $m_e = e = \hbar = \frac{1}{4\pi\epsilon_0} = 1$. Consequently, all the energies will be expressed in Hartrees (1 H = 27.2114 eV) and all the distances in Bohr radii (1 a_0 = 0.529 ångström).

2.1 Density Functional Theory

The aim of this theory is to obtain a computable set of equations from the time-independant Schrödinger one (Eq 2.1). It will be shown that even with as many approximations as can be done, the Schrödinger equation is still too expensive computationally.

$$H\Psi(x_1, x_2, \dots) = E\Psi(x_1, x_2, \dots) \quad (2.1)$$

$$H = T + T_n + V_{ee} + V_{nn} + V_{ext}$$

Where $\mathbf{x}=(\mathbf{r},\sigma)$, \mathbf{r} being the coordinate and σ the spin. Each electron, proton and neutron has then 6 degrees of freedom. T is the kinetic energy of the electrons, T_n the kinetic energy of the nucleus, V_{ee} the interaction energy between the electrons, V_{nn} is the interaction energy between the nucleons and V_{ext} is the external potential. In the case of materials simulations, and so in the context of this thesis, the external potential is due to the interaction between the electrons and the nuclei. It is considered that no other potential is applied. From these equations can be seen that two parameters have to be determined: the Hamiltonian and the wavefunction.

2.1.1 Hamiltonian

In the Born-Oppenheimer approximation, the nucleus is considered as motionless since it is much heavier and much slower than the electrons [14]. It can then conveniently be considered that T_n is zero and V_{nn} is a constant. Doing this, the Hamiltonian can be separated into one Hamiltonian for the electrons and one for the nuclei. Electronwise, the Hamiltonian is now described in equation 2.2. This Hamiltonian is the one containing the physics of interest for this work.

$$H = T + V_{ee} + V_{ext} \quad (2.2)$$

2.1.1.1 Hartree-Fock (HF)

The ground state of a system can be found from the Hamiltonian by finding the wavefunction that minimizes the average total energy, using the variational principle (Equation 2.3). In this equation, Ψ has to be antisymmetric and normalized.

$$E[\Psi] \geq E_0 \quad (2.3)$$

For non-interacting systems, Hartree-Fock proposed the following ansatz.

$$\Psi(\mathbf{x}_1, \mathbf{x}_2, \dots, \mathbf{x}_N) = \frac{1}{\sqrt{N!}} \begin{vmatrix} \psi_1(\mathbf{x}_1) & \psi_2(\mathbf{x}_1) & \cdots & \psi_N(\mathbf{x}_1) \\ \psi_1(\mathbf{x}_2) & \psi_2(\mathbf{x}_2) & \cdots & \psi_N(\mathbf{x}_2) \\ \vdots & \vdots & & \vdots \\ \psi_1(\mathbf{x}_N) & \psi_2(\mathbf{x}_N) & \cdots & \psi_N(\mathbf{x}_N) \end{vmatrix} \quad (2.4)$$

This wavefunction is a Slater determinant. It is antisymmetric (conform to the Pauli principle) and normalized. Each ψ depends on only one electron. N is the total number of electrons in the system. Using this wavefunction in the Schrödinger equation yields the Hartree-Fock equations.

$$\left[-\frac{1}{2}\nabla^2 + \nu_{ext} + \int \frac{\rho(r')}{|r-r'|} dr' \right] \Phi_i(r) + \int \nu_X(r, r') \Phi_i(r') dr' = \epsilon_i \Phi_i(r) \quad (2.5)$$

$$\int \nu_X(r, r') \Phi_i(r') dr' = - \sum_j^N \frac{\Phi_j(r) \Phi_j^*(r')}{|r-r'|} \Phi_i(r') dr' \quad (2.6)$$

Where ν_X is the non-local exchange potential.

The Hartree energy is different from the exact energy by about 20 to 40 mH/electron [15]. This difference is called the correlation energy and is due to the non interacting kinetic energy and to the only approximated external potential.

Better approximations exist, but solving these equations requires times increasing to the power of 5 to 7 with the number of electrons. It is easily understandable that it cannot be used for system with hundreds of electrons.

Instead, the DFT theory has been developed.

2.1.1.2 The Hohenberg Kohn (HK) theorems

Hohenberg and Kohn made the really simple and really powerful following statement [16].

“The external potential $v_x(r)$ is (to within a constant) a unique functional of the ground state electron density $n(r)$.”

If the electron density determines the external potential, it is quite straightforward from Equation 2.2 that the electron density also determines the Hamiltonian and hence all the properties which are directly derived from the Hamiltonian.

The second statement from Hohenberg and Kohn was that “ $E(n)$ assumes its minimum value for the correct $n(r)$ with $\int n(r) dr = N$.”

It means that finding the ground state density enables to deduce the ground state energy. However, we still have to find three functionals at this point. If the interaction with the external potential is easy to find, the kinetic energy and the electron-electron interaction functionals are much harder to express, and research on that topic have not met success yet.

2.1.1.3 Kohn and Sham

It is nevertheless possible to get round these issues by defining another system, with the same electron density, no mutual interaction, and a different external potential to compensate [17]. Since there are no interaction, it is possible to define in an exact way the kinetic energy and the density.

$$T_s[\rho] = -\frac{1}{2} \sum_i^N \langle \Phi_i | \nabla^2 | \Phi_i \rangle \quad (2.7)$$

$$\bar{\rho}(r) = \sum_i^N |\Phi_i|^2$$

For the electron-electron part, Kohn and Sham distinguished the classical Coulomb interaction and the non-classical repulsion energy, which is composed of the exchange and the correlation of Coulomb, and the self-interaction correction. The classical part, or Hartree energy is defined as

$$V_H = \frac{1}{2} \int \int \frac{\rho(r_1)\rho(r_2)}{|r_1 - r_2|} dr_1 dr_2 \quad (2.8)$$

The factor $\frac{1}{2}$ accounts for the fact that each interaction is counted twice.

However, only a part of the electron-electron interaction is calculable, and the kinetic energy is not completely the same as in the interacting system. It is then necessary to define the exchange-correlation energy to make up for the difference as

$$E_{xc}[\rho] = T[\rho] - T_s[\rho] + V_{ee}[\rho] - V_H[\rho] \quad (2.9)$$

where T and V_{ee} are the kinetic and electron-electron interacting energy in the real system and T_s and V_H are defined in the Kohn Sham system.

This exchange-correlation energy is unknown and is composed of

1. The correlation between two electrons of same spin (Pauli principle)
2. The self-interaction correction
3. The Coulomb correlation for electrons of opposed spin
4. The difference in kinetic energy between the interacting and the non interacting systems

From the Hartree-Fock equations (Equation 2.5), applied to this new system, the Kohn-Sham equations can be derived.

$$\left[-\frac{1}{2}\nabla^2 + \nu_{ext} + \int \frac{\rho(r')}{|r-r'|} dr' + \nu_{XC}(r) \right] \Phi_i(r) = \epsilon_i \Phi_i(r) \quad (2.10)$$

$$\nu_{XC}(r) = \frac{\delta E_{XC}[\rho]}{\delta \rho}$$

The idea to solve the problem would be to follow this iterative scheme: first, an electronic density is stated. From this density, all the functionals are determined, which allows us to solve the Kohn-Sham equations. This gives the new orbitals, and a new density is calculated. This algorithm is running until the density converges. It is illustrated in Figure 2.1.

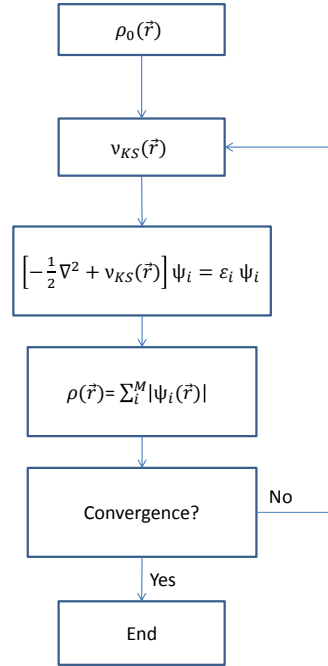


Figure 2.1: Flow-chart of a typical DFT calculation within the Kohn-Sham framework.

It is worth noting that until now, the equations are exact. Unfortunately, the real exchange-correlation energy is not known and it is necessary to make some approximations here. These approximations have to be precise and not to require too much calculation power. Over the past few years, a

lot of different methods have been proposed, some of which, used or leading to the ones used in this work, are presented now.

2.1.1.4 The Local Density Approximation (LDA)

This approximation states that the exchange correlation energy of the system is locally determined only by its electronic density. To each point of space is corresponding a density and therefore an exchange-correlation energy. This is the simplest approach, which find root in the 1920's. Indeed, most of the LDA approaches have been derived from the Homogeneous Electron Gas theory of Thomas-Fermi. Under this hypothesis, the kinetic and exchange energies for non-interacting system are known.

$$T[\rho] = 2.87 \int \rho^{5/3}(r) dr \quad (2.11)$$

$$E_X[\rho] = 0.74 \int \rho^{4/3}(r) dr$$

Finding the correlation energy is harder and numerous different attempts exist (VWN, PZ81, CP, PW92, ...). The LDA approximation gives strikingly accurate results due to a cancellation of different errors [15][18]. However, it is possible to find a better approximation without increasing too much the calculation time.

2.1.1.5 The Generalized Gradient Approximation (GGA)

This approximation extends the LDA by considering the surrounding electronic density before calculating the exchange correlation energy in a specific place. The exchange-correlation energy is then described as in equation 2.12.

$$E_{XC} = \int \rho(r) \epsilon_{XC}(\rho, \nabla \rho) dr \quad (2.12)$$

For this kind of functionals, the pragmatism is favored over the physical meaning. The functional is modified in an arbitrary way to respect the boundary conditions, and only its performance matters. This conducted Koch and Holthausen to say that “Some of these functionals are not even based on any physical model” [19].

Again, a lot of different functionals have been developed (PW91, PBE, B3LYP) and have advantages and drawbacks depending on the properties of interest [18].

To go even further, some functionals take into account the second derivative of the electronic density (Meta-GGA functionals), or mix a non-interacting approach with a fully interacting one (Hybrid Exchange Functionals).

2.1.1.6 The Perdew Burke Ernzerhof potential (PBE)

The Perdew Burke Ernzerhof potential is a modified GGA potential in which all parameters are fundamental constants [20]. It is a simplification of the PW91 potential which fits only the most relevant conditions on an energy level and is hence easier to understand, derive, and implement. This functional keeps the correct properties from the LDA and adds others such as superior limits for the exchange and the correlation energies but neglects a few aspects, including the second order gradient coefficients for E_X and E_C in the slowly varying limit. The choice of the correct properties has been made depending on what seemed the most important on an energy level.

The PBE potential is the one that has been used for all the simulations in this thesis, using the potential data bank of VASP.

2.1.2 Wavefunctions

Having good representations of the wavefunctions is essential since they are used in the iterative process to determine the density. Hence, they have to be as precise as possible. However, determining a good way to represent the wavefunctions can be tricky, this representation having to be both realistic and computationally efficient in any part of space.

In this work, the Projector Augmented Wave method has been used. Various papers can be consulted for more information [21][22].

2.1.2.1 Pseudopotential methods

These methods use plane waves, as defined by equation 2.13.

$$\Phi_i(r) = \sum_K c_{i,K} e^{i(k+K).r} \quad (2.13)$$

If fitting the real wavefunction with plane waves is really computationally efficient in the areas far from a nucleus, it needs a huge basis set in the core region to be convergent, since the real wavefunction varies quickly. However, most of the physical properties are defined by the valence electrons and the nuclei part can be thought as not changing in different environments (frozen core approximation). For this reason, the pseudopotential method consists in fitting to the reality in the valence region, but modifying the wavefunction in the core region to soften it (Figure 2.2) and fasten the convergence.

The cut-off radius (r_c) has to be chosen such as the potential is converging quickly (higher radius) but is still usable for systems with a different

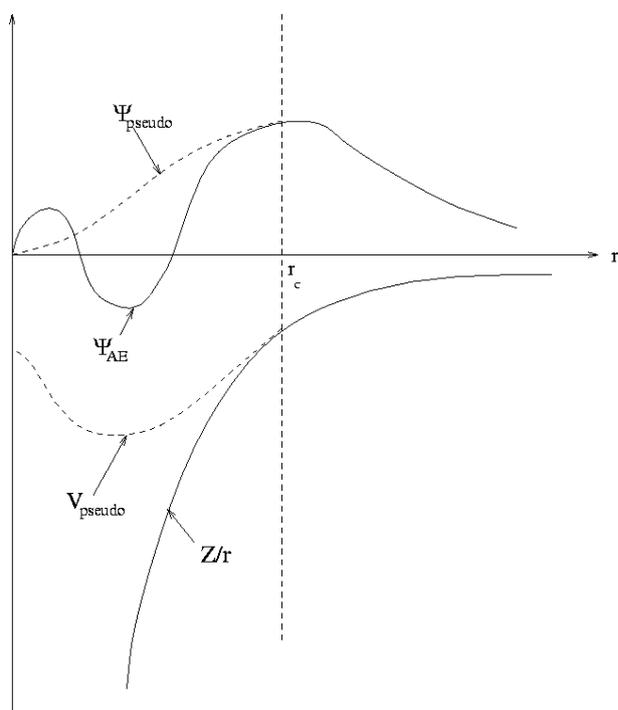


Figure 2.2: Illustration of the pseudopotential and of the pseudo wavefunction.

environment, that is to say that the unvarying frozen core should not be too big (lower radius).

The main advantage of this method is to reduce the number of electrons of interest, considering only the valence ones, and doing so, increasing the size of a studied system for the same computation time. Another advantage is to reduce the basis set size, and therefore to speed up the calculations. However, these wavefunctions should be norm-conserving and ultrasoft pseudopotentials, which don't have to respect this condition, have been proposed by Vanderbilt [23] to further reduce the basis set.

2.1.2.2 Augmented Wave methods

Augmented Wave methods are based on the muffin-tin approximation. This approximation divides space in two: Spheres of radius s centered on the atom positions, and in which the potential is the average radial value, and the interstitial zone, in which the potential is constant.

$$V(r) = \begin{cases} V(r) & \text{if } r \leq s \\ V_0 & \text{if } r \geq s \end{cases} \quad (2.14)$$

Due to symmetry reasons, the wavefunction in the sphere is

$$\Psi^1 = \sum_{l=0}^{\infty} \sum_{-m}^m a_{lm} U_l(r) Y_{lm}(r) \quad (2.15)$$

Where Y_{lm} are the atomic orbitals and U_l can be found with

$$\left\{ \frac{d^2}{dr^2} + \frac{l(l+1)}{r^2} + V(r) - E \right\} r U_l(r) = 0 \quad (2.16)$$

In the interstitial region, the potential is constant. The wavefunction is then a plane wave serie (Equation 2.13). Saying that the two wavefunctions are equal at $r=s$, the a_{lm} coefficients can be determined using Bessel orbitals.

This wavefunction is a solution for one atom. To have a solution for the whole crystal, it is necessary to use a linear combination of these wavefunctions. The augmented wave is then:

$$\Psi_k(r) = \begin{cases} \sum_{l=0}^{\infty} \sum_{-m}^m A_{lm}(k+K) U_l(r) Y_{lm}(r) & \text{if } r \leq s \\ \Phi_i(r) = \sum_K \frac{c_{k+K}}{\sqrt{\Omega}} e^{i(k+K).r} & \text{if } r \geq s \end{cases} \quad (2.17)$$

2.1.2.3 Projector Augmented Wave method (PAW)

It is a mix between the pseudo potential and the augmented wave methods. In the core region, the wavefunction is expressed with the help of the atomic orbitals (from the augmented wave method) and in the valence zone, plane waves are used (from the pseudopotential method). This allows an equivalent speed of calculation with more precise results.

To avoid having to calculate two sets of wavefunctions, auxiliary wavefunctions which can get derived from the real wavefunctions by a linear transformation are used. This linear transformation is such that in the valence region it becomes the identity. In the core region, the real wavefunctions can be obtained by adding to the identity the projection of the auxiliary set on the atomic orbitals of the atom with all its electrons, and subtracting the same projection on the atomic orbitals of an atom with just the valence electrons, to avoid counting it twice (once from the identity, once from the projection).

$$|\psi_n\rangle = |\tilde{\psi}_n\rangle + \sum_a \left(\sum_i |\phi_i^a\rangle \langle \tilde{p}_i^a | \tilde{\psi}_n\rangle - \sum_i |\tilde{\phi}_i^a\rangle \langle \tilde{p}_i^a | \tilde{\psi}_n\rangle \right) \quad (2.18)$$

where ψ_n and $\tilde{\psi}_n$ are the real and auxiliary wavefunction, ϕ_i^a and $\tilde{\phi}_i^a$ the atomic orbitals of the atom with all the electrons and with only the valence electrons, \tilde{p}_i^a is the projector, and a represents the atoms.

2.1.3 Vienna Ab-initio Simulation Package

For all the DFT calculations in this work, the Vienna Ab-initio Simulation Package (VASP) has been used. The chosen potentials are PBE used with the Projector Augmented Wave method. The energy cut-off for the basis set has been chosen to be 450 eV due to the presence of oxygen in the systems of interest. It has been shown that there is no significant change when this cut-off is set to an higher value, except for a much larger calculating power required.

VASP uses periodic boundary conditions, that is to say that the supercell repeats itself. Again, it is important to choose a supercell big enough to avoid too big boundary effects, but it has to be small enough so it will not take an unreasonable time to reach convergence. Unless otherwise specified, the simulations have been made using a supercell of 250 base atoms and a sampling of the Brillouin zone with 27 points. To help convergence, an electronic temperature has been used (through the parameter SIGMA, 0.3

in this work). These parameters have been chosen high enough to reach a convergence of the free energy and low enough to keep a calculation time under 24 hours.

Most of the simulations have been run in two steps, one to reach a near-convergence state with specific parameters to accelerate the simulation while loosing some accuracy, and one to converge and obtain accurate data from this state with the above-mentioned parameters.

2.1.3.1 Nudged Elastic Band (NEB) method

In order to simulate a dynamic system, it is necessary to find data for the diffusion of atoms. This value is the migration energy and is found by computing the minimum energy path (MEP) between two stable configurations. It is found combining the density functional theory with the nudged elastic band method. It would have been possible to use other methods [24], such as the slowest ascent path [25] (drag method).

The idea with the NEB (chain-of-states method) is to calculate the equilibrium state of the system in an initial and a final geometric configuration using a DFT code. Then, a certain amount of images are created, moving progressively the atoms which are not in the same position in the two states. This motion is linear in function of the number of images asked. In figure 2.3 are shown two images between one state with a blue atom first nearest neighbour from a vacancy and a final state where both of them have exchanged their positions. Obviously, the vacancy is not physically moving, since it represents an absence of atom.

Once the images are defined, a DFT calculation is run for each of them, and they are relaxed. However, they are constrained by strings, which force the distances between each other to remain equal [26]. This is done by projecting out the perpendicular component of the spring force and the parallel component of the true force [27].

2.2 Kinetic Monte Carlo

One of the main drawbacks of the DFT is that the time scale is limited to a few nanoseconds, and the length scale to few nanometers. It is then necessary to use another method to have results for a longer time or a bigger material. Numerous ways of doing so exist (FIG 2.4), but in this thesis, a kinetic Monte Carlo code has been used.

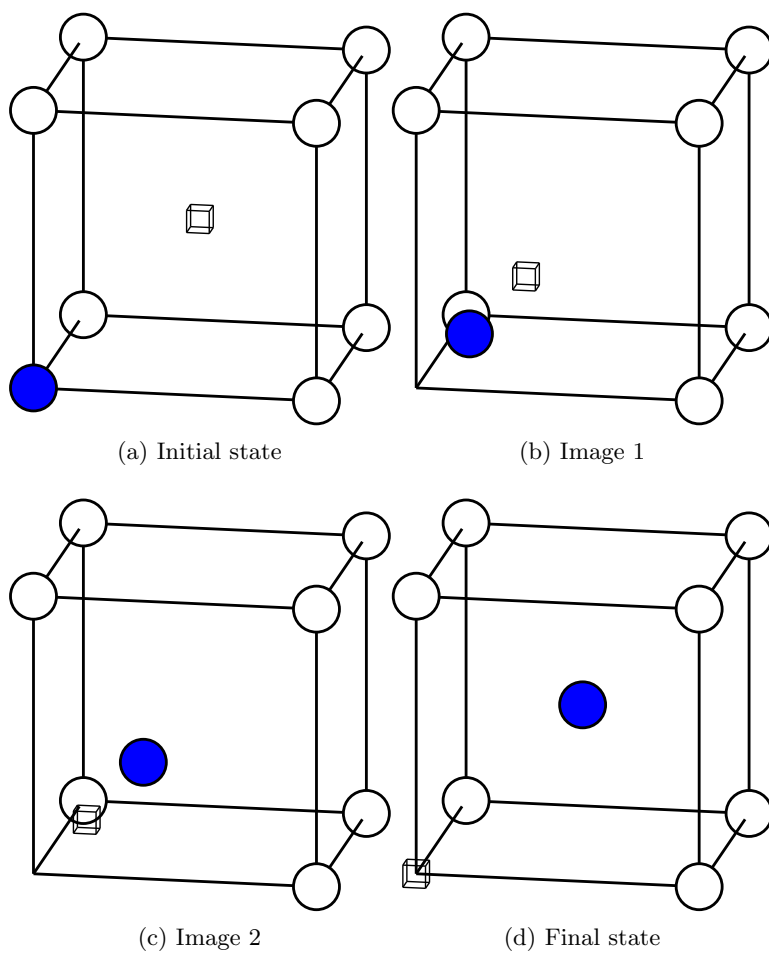


Figure 2.3: Illustration of the images in the NEB method

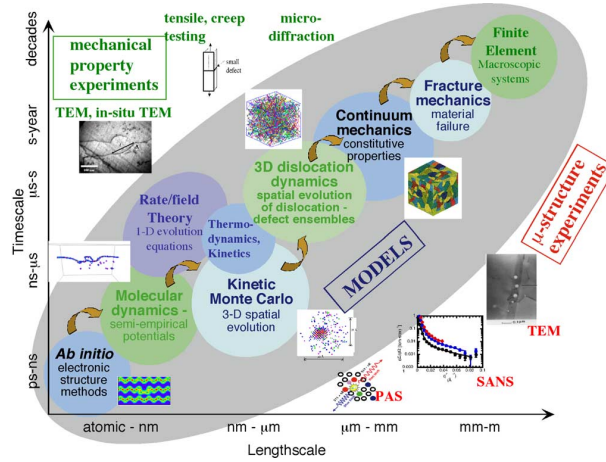


Figure 2.4: Map of the simulation methods depending on the aimed timescale and lengthscale.

A Monte Carlo code is based on random choices of possibilities. Repeating the event, one can get better statistics, until the results become reliable. A classic example of a Monte Carlo application is to determine π . In a 1 unit-sided square, a circle of radius one half unit is drawn. Then, a random process picks two numbers between zero and one. These numbers are the coordinate of the point. π is four times the ratio between the number of points in the circle and the total number of points. It is obvious than after one event only, it will gives $\pi = 0$ or 1, but after an infinity of events, the result will be exact. Therefore, for any Monte Carlo simulation, one has to find a compromise between speed and accuracy.

Number of events	1	10	1000	100000	10000000
Value of π	0	2.8	3.084	3.13644	3.14107

Table 2.1: Value of π given by a MC process depending on the number of events

It works exactly the same way when it comes to point defect simulations. A given vacancy has probabilities to exchange position with a few atoms. A random number is picked, and this number will decide which jump will be done. The probabilities are given thanks to a model describing the interactions between the atoms.

2.2.1 Atomic Kinetic Monte Carlo

A atomic Monte Carlo methods means that the different atoms are bound to the lattice positions. One have to be aware that this method doesn't support high disturbances of the lattice. It could be a problem here since some of the nanoclusters studied have a completely different lattice parameter than the one of α -iron, but since these clusters keep a small size in the nucleation stage, the condition is supposed to be met [11].

To have a notion of kinetics one needs a time-step, which in this method is defined as the inverse of the sum of the migration probabilities by second, given by the residence time algorithm. The theoretical determination of the time-step is usually done in the framework of the Transition State Theory [28]. In this framework,

$$\Gamma_{X,V} = \nu_X \exp\left(-\frac{E_a}{kT}\right) \quad (2.19)$$

where Γ is the migration probability by second, that's to say the probability that an atom and a vacancy V exchange their positions during the step X, ν is the attempt frequency which depends on the type of atom and the temperature, k is the Boltzmann constant, T the temperature and E_a the activation energy for the jump defined (Eq 2.20) and modeled (Eq 2.21) as

$$E_a = E_{SaddlePoint} - E_i. \quad (2.20)$$

$$E_a = E_m^* + \frac{E_f - E_i}{2}. \quad (2.21)$$

E_m^* is the migration energy of a vacancy with the first neighbour atom. One is defined for each type of atom and for the jump of an interstitial atom; For the case of oxygen, the migration energy is defined between two first nearest neighbour octahedral positions. E_f and E_i are the final and initial energies. This equation allows us to not need to calculate every migration energy with a Nudged Elastic Band (NEB) method, which would be time-prohibitive.

ν can be determined with a relative precision by

$$\nu = \frac{\prod_i^N \omega_i^{start}}{\prod_i^{N-1} \omega_i^{saddle}} \quad (2.22)$$

where ω_i^{start} and ω_i^{saddle} are the frequencies of the entire system at equilibrium and the frequencies of the entire system except the jumping atom when this one is at the saddle point. Usually, ν is around 10^{-12} .

The time-step for one vacancy at one step can then be calculated as

$$\Delta t_{X,V} = \frac{1}{\sum_{X,V} \Gamma_{X,V}} \quad (2.23)$$

However, the system has to be at the thermodynamical equilibrium for this formula to be usable. Unfortunately, the equilibrium concentration of vacancies is so low that even with only one, the system is over saturated. The time-step has to be corrected to account for this.

$$\Delta t' = \frac{C_V}{C_V^{eq}(T)} \Delta t \quad (2.24)$$

where the equilibrium concentration of vacancies at the temperature T can be found using the Gibbs energy (Eq 2.25 [29]) and $\Delta t'$ is the corrected time-step.

$$C_V^{eq}(T) = e^{-\frac{G_f}{k_b T}} \quad (2.25)$$

where k_b is the Boltzmann constant and G_f is the Gibbs energy of vacancy formation.

2.2.2 LAttice KInetic MOnte CARlo

In the context of this thesis, the Monte Carlo code used is LAKIMOCA (LAttice KInetic MOnte CARlo). It is written by C. Domain at Électricité de France. It was started in 1998 and is still under development.

This code can read numerous types of potential, and the one used here was of type Embedded Atom Model [30]. It has been run using an iron lattice of 42*42*42 cells, with chromium, titanium, yttrium in substitutional positions, oxygen atoms in octahedral positions and one vacancy.

For each step, the code will consider the vacancies, the Self Interstitial Atoms (SIA) and the Foreign Interstitial Atoms (FIA) and calculate the probabilities of these to jump, depending on the surroundings. Then, it will randomly pick a jump for each of those. Once this has been done for all the defects, a new step is launched.

The other parameters are the jump attempt frequency, the temperature, the lattice parameter, the number of steps and a seed for the random number generator.

2.3 Materials irradiation

2.3.1 Defects

During the lifetime of a material, several types of defects can occur in the crystal lattice. It is especially true if this material undergoes irradiation. They are generally classified by their dimension, from 0 (point defects) to 3 (space defects). We can briefly mention the most relevant of them in the context of this thesis.

The first kind of defect we can mention comes from the very composition of a crystal. There are always impurities. Their concentration can vary a lot but will never be zero. If these impurities occupy the normal lattice position, they are referred to as substitutional atoms. Otherwise, they are called Foreign Interstitial Atoms (FIA) and stay in the interstitial positions, most often octahedral and tetrahedral sites. These sites can also be occupied by the crystal atoms which are in this case known as Self Interstitial Atoms (SIA).

On the contrary, sometimes there exist normal lattice positions which are not occupied. They are called vacancies. Vacancies and self interstitial atoms can recombine and in this case, both defects are destroyed.

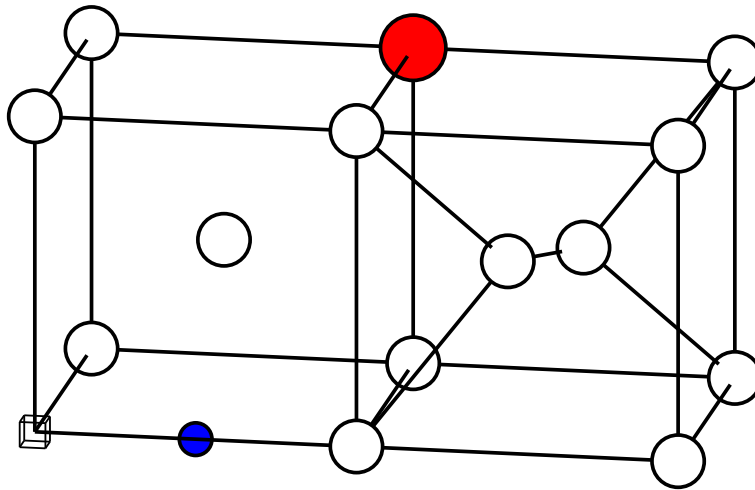


Figure 2.5: Different types of defects in a crystal

In figure 2.5 are represented a vacancy in $(0;0;0)$, a FIA in blue, a substitutional atom in red, and a SIA around the lattice position $(1.5;0.5;0.5)$.

When several of these defects gather in a small region of the crystal, being under the influence of each other, they become a cluster. Clusters

can dramatically modify the mechanical behaviour of a material, as will be explained more in details in part 2.3.3.

This work is mainly aimed on these point defects, but also dislocations [31], grain boundaries [32] and clusters can be mentioned.

2.3.2 Energies

In the context of this thesis, the point defects have been well studied. To do that, it is necessary to define some energies. These energies will give information on if a crystallographic configuration is stable or if a transformation is thermodynamically favoured. As such, it is crucial to have a precise definition for each.

- The cohesive energy: it is the difference between the energy of a solid and the energy of the isolated atoms. It represents the force acting against the separation of the atoms. It can be calculated thanks to the following formula.

$$E_{coh} = E_{tot} - \sum_N E_{iso} \quad (2.26)$$

- The binding energy: When there exists more than one defect in a lattice, one can quantify the influence of one defect on the other one. To do so, the energy associated to the neighbouring of these two defects is calculated (Eq. 2.27) as the difference between the energy of a crystal where the defects are close and the same crystal where the defects are far from each other.

$$E_b = E_{tot_A} - E_{tot_B} \quad (2.27)$$

Where the configuration A is the one with the defect close and the B is the one with far from each other defects.

However, since for computational reasons, it is not always possible to put defects at a long enough distance to consider that they have absolutely no effect on each other, the Eq. 2.28 is often used. The defects are taken alone in an otherwise perfect lattice. The result is the same as if it was possible to set the defect at an infinite distance in the same system.

$$E_b = E_{tot} + E_{ref} - E_{defect1} - E_{defect2} \quad (2.28)$$

This equation can be generalized to N defects as

$$E_b = E_{tot} + (N - 1)E_{ref} - E_{defect1} - E_{defect2} - \dots - E_{defectN} \quad (2.29)$$

- The migration energy: To simulate the kinetics of a system, the migration energy is an important value. It represents the barrier that an atom needs to pass in order for the system to go from one stable state to another. Stable positions have local energy minima and therefore, the energy of the atom will be higher on the migration path. We call the saddle point the point where the atom have the highest energy on the path of lowest energy. The difference in energy between the saddle point and the starting point is the migration energy. The saddle energy is found by determining the MEP, thanks to methods such as the NEB one.

2.3.3 Macroscopic effect of irradiation

Under irradiation, due to the high energy neutron flux received by the material, there is a multiplication of point defects. Indeed, the energy of the incoming neutrons is several orders of magnitude greater than the threshold displacement energy of the atoms (order of magnitude of 1 MeV for the neutron against several tens of eV for the threshold) and so, each neutron will generate a collision cascade in the material, resulting in the creation of numerous defects such as Frenkel pairs, which number is estimated in equation 2.30 [33]. Most of these defects will recombine and only 20% to 30% will survive [34], but the remaining ones will drastically change the macroscopic properties of the material. Among various effects which can be read more in details in Recent Development in Irradiation-Resistant Steels [35], some deserve to be mentioned.

$$N_{FP} = 0.8 \frac{E_n}{E_{Tres}} \quad (2.30)$$

where N_{FP} is the number of Frenkel pairs, E_n and E_{Tres} are the neutron energy and the threshold displacement energy.

2.3.3.1 Swelling

Swelling in structural materials is a major problem in reactors since it will limit the performances of the reactor core. It will occur in two steps; the first one, or incubation stage, is quite slow and is due to the cavity formation

and grain growth. This phase duration depends on various parameters like the temperature or the dose rate. The solute concentrations also play an important role and will be further detailed. The second phase is faster and causes a swelling of about 1% per dpa (Displacement Per Atom: 1 dpa means that every atom has been moved from its initial position once on average) for stainless steels due to the formation of helium bubbles. The incubation period has been observed to be the shortest at around 750 K for a SS316 steel (Table 2.2) and stops for doses of 35-40 dpa [36].

Composition	Cr	Ni	Si	Mn	P	S
SS316[37]	17	12	1	2	0.045	0.030
MA957[38]	14	0.13	0.04	0.08	0.015	0.006
EUROFER[39][40]	9	0.005	0.05	0.4	<0.005	<0.005
composition	Ti	Y	O	Mo	W	C
SS316	NA	NA	NA	2-3	NA	0.08
MA957	0.9	0.2-0.3	0.22	NA	0.014	NA
Eurofer	NA	NA	NA	0.005	1.1	0.11

Table 2.2: Composition of some steels in weight %.

Concerning the composition, it can be said that the presence of nickel will increase the swelling due to the probable (n,α) reaction and that titanium has the opposite effect and reduce swelling, as well as phosphorus [41]. The addition of around 6% of chromium also dramatically reduce swelling [42]. Nevertheless, austenitic steels will in the best case be able to handle 120 dpa before the swelling induced embrittlement reaches a critical limit after a swelling of 3% [43]. After this limit, Porollo et. Al. showed that fracturing of the fuel elements and a degradation of the cladding properties occur. Ferritic-martensitic steels can resist 200 dpa.

2.3.3.2 Ductile to Brittle Transition Temperature (DBTT) shift

A material can be ductile or brittle. If it is ductile, it will deform before breaking, which will not be the case if it is brittle. This results in a difference in the impact energy measured by Charpy testing, which quantifies how much energy can be absorbed by a material before failing. Even if the neutron-induced embrittlement can cause an hardening of the material, the exact properties can not be known and a ductile behaviour is hence wanted.

The problem here is that irradiation causes a shift of the DBTT and a material which is originally ductile can become brittle after a few years. The order of magnitude of the shift for an EUROFER steel (see table 2.2) is of 200-250 K for dpa ranging from 30 to 80 at around 600 K. The dose rate is not indicated [36]. Austenitic steels have on this point a huge advantage since they will stay ductile at room temperature until after the swelling becomes an issue. On the other hand, ferritic-martensitic steels will become brittle after a few dpa. This problem is exacerbated for low irradiation temperature but can be reduced with a concentration of 9% of chromium [36] as it is shown on picture 2.6. The presence of Ni leads to a larger amount of He atoms in the iron matrix under irradiation, which causes a larger shift of the DBTT [44].

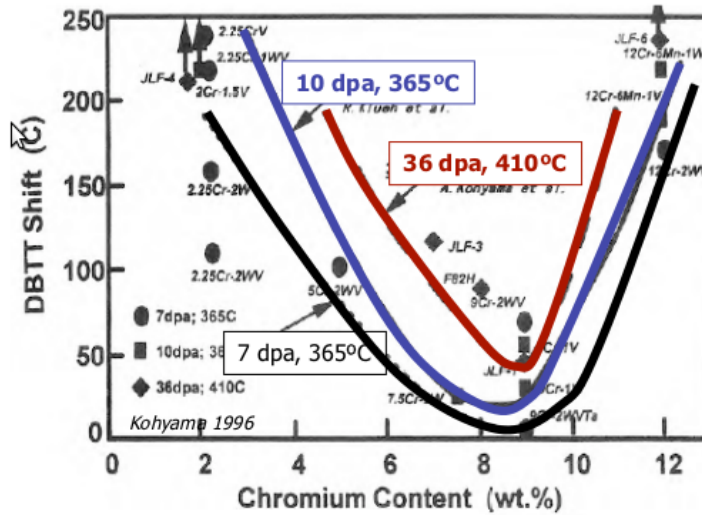


Figure 2.6: Influence of the chromium content on the DBTT shift.

2.3.3.3 Creep rupture embrittlement

When a material undergoes irradiation, its resistance to creep progressively decreases. The creep rupture time can be expressed in function of the pressure and the temperature as

$$P = T(A + \log(t_r)) \quad (2.31)$$

where T is the temperature in kelvin, t_r is the rupture time, P is the

Larson-Miller parameter and A is a constant. Both P and A depends on the pressure and on the material.

The creep rupture time is much longer for austenitic steels than for ferritic-martensitic steels and decreases when the irradiation is done at high temperature [36][45]. The creep resistance can also be enhanced by the addition of W and Nb [46].

2.3.4 Oxide Dispersion Strengthened (ODS) steels

As seen in the previous part, both austenitic and ferritic-martensitic steels have resistance problem when they are under irradiation for a long time, and this no matter what the temperature is. Efforts that have been made to change the composition including for instance titanium or chromium have given reasonably good results, but this is still not satisfying for GEN IV fission or fusion usages. However, the three above mentioned issues can be significantly reduced by the use of ODS steels.

2.3.4.1 Principle

The principle here is to add to the steel some other atoms, which will create a large amount of nano-scaled precipitates, around $10^{24}.m^{-3}$ [47]. The steel and the wanted components of the nanoclusters are mechanically alloyed (MA) by ball milling. Typically, the created nano-ferritic alloy will contain yttrium, titanium, tungsten, chromium and oxygen.

The chromium is useful to increase the resistance of the steel to oxidation and corrosion, while the tungsten will be beneficial to improve the strength of the steel, forming solid solutions. Yttrium, titanium and oxygen cluster and prevent dislocations from moving. Titanium can be replaced by zirconium for a higher stability [7]. Depending on the composition of the alloy and of the temperature of the heat treatments, nanoclusters are ranging between 1 nm and 2 nm of radius, and have a volume fraction between 0.4% and 2%. The composition of the clusters can also vary from near equilibrium oxides like Y_2TiO_5 or be a bit further, like $Y_2Ti_2O_7$ or Y_2TiO_3 [35].

2.3.4.2 Known results

When not under irradiation, the ODS steels exhibits a high tensile and creep strength and a rather good tensile ductility. Their low-cycle fatigue properties are also excellent [35]. However, the behaviour under irradiation is what is of main interest.

It has been found that irradiation -up to 150 dpa at 975 K and 10^{-3} dpa/s using 6.4 MeV Fe^{3+} ions- doesn't affect significantly nanoclusters [48]. A prolonged exposure to high temperature doesn't cause coarsening even after 14500 hours at 800°C [47].

Those nanoclusters trap helium that is generated into small bubbles and prevent the material from swelling in a significant way [49]. Thus, the swelling induced embrittlement is reduced. The very high density of nanofeatures as well as the obstacles due to irradiation trap the dislocation loops. Due to this pinning, the dislocation density is 10 times higher compared to the ODS steels without (Y,Ti,O) clusters and the creep rate at around 1000 K is reduced by 6 orders of magnitude [47]. Losses of ductility due to irradiation are also reduced compared to martensitic steels [50], and the presence of Cr in the ODS steel reduces the shift further [51].

Chapter 3

Results

In this section are reported the results of this thesis. They are divided into two parts; the ones coming from the ab initio calculations and the ones coming from the Monte Carlo simulations.

In the first-principles chapter, the focus is first given on finding the stable position for each considered atom in a BCC iron lattice. Then, the interactions between the solutes and the vacancies are treated. In the following part, migration energies are computed. Thereafter, interactions between two solutes will be studied. From all of these data, the possibility of forming a cluster and simple mechanisms for the formation will be discussed. The peculiar attraction of oxygen atoms toward a vacancy as well as the unexpected diffusion mechanism for the yttrium atom will be developed in more details.

Then, in the atomistic kinetic Monte Carlo part, all the parameters from the ab-initio simulations will be used to

- study the formation of nanoclusters
- study the stability of these clusters under normal conditions

3.1 Ab-initio calculations

These ab initio simulations (described in the theoretical background part) only depend on the choice of approximations for the Hamiltonian and for the wavefunctions. Hence, a good accuracy can be expected for the results. All these first-principles calculations have been made using VASP, and the details about the configuration are given in the section 2.1.3, and have been chosen so that a convergence is reached. The simulations of this work are supposedly more precise than what can be found in the literature since the

sampling of the Brillouin zone is denser, the supercell bigger and the energy cut-off higher.

One has to be aware that all of the data presented in this part are only valid in the dilute limit. When the concentration of a solute becomes too high, new phenomena start and modify the behaviour of the solute. For instance, Cr will cluster if its concentration is higher than a few percents.

3.1.1 stable position of solutes

In order to calculate the binding energies between two defects in the iron lattice, it is necessary to have the solution energy of these solutes in the stable position. To do that, the cohesive energy of each atom is calculated either in the reference crystal (for Cr, Ti and Y) or in a dimer (for O) and are listed in table 3.1. The stable position can be found trying to put the atom in different sites and checking for which the energy is the lowest. On the figure 3.1 are the tensile (in red), compressed (in blue) and mixed (in green) site of a cell when there is a self interstitial atom (SIA) in the plane $[110]$, as described by Olsson et. Al. [5].

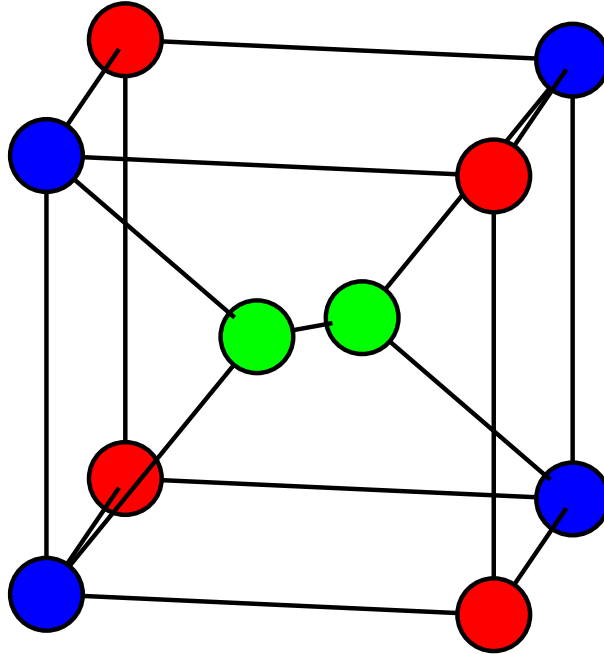


Figure 3.1: Tensile, compressed and mixed sites.

These configurations have been found more stable for iron than the ones with an SIA in the octahedral or tetrahedral sites. It is worth being explored

for Ti, Cr and Y also. The values found are reasonably close from the literature, which confirms the model. An exception to that is the oxygen data. However, no-one in the literature explains where the cohesive energy they use has been found. In this work, a magnetic dimer has been used. Using a different cohesive energy can lead to different solution energies, but these values are not primordial for the next steps, since a difference in energy is used to calculate any binding energy. For this reason, the comparison criteria should be the difference in energy between the octahedral and the tetrahedral sites. It can also be noticed a big difference with C. C. Fu values which seem a bit under-evaluated, probably due to the fact that she used a different code.

The results shown in the table 3.1 prove that Ti, Cr and Y are more stable in a substitutional site and oxygen is found more stable in the octahedral site, by 0.51 eV compared to the tetrahedral position in confirmation of Murali's work and infirming Jiang's one where a mistake has probably been made. The binding energies are also indicated in table 3.2 for a SIA and a substitutional solute. The only attractive one is the tensile, which was expected since the [110] dumbbell makes the compressed sites closer and the tensile sites further from the SIA than if there was no defect.

Element	Fe	Cr	Ti	Y	O
Cohesion (eV/at)	8.31	0.00 ^b	7.61	6.26	4.92
Substitutional	-	-0.12 ^b	-0.92 (-0.80 ^c)	2.01 (2.02 ^c)	-(2.99 ^c , 3.01 ^d)
Octahedral	5.36 (4.94 ^a , 5.29 ^b , 5.27 ^c)	4.88 ^b	-	-	-0.38 (1.41 ^c , 1.35 ^d)
Tetrahedral	4.54 (4.26 ^a , 4.44 ^b , 4.45 ^c)	4.26 ^b	-	-	0.13 (3.26 ^c , 1.76 ^d)
Compressed	4.08 (3.64 ^a , 4.02 ^b , 4.04 ^c)*	3.86 ^b	3.53 (3.80 ^c)	6.80 (6.24 ^c)	-
Tensile		3.98 ^b	3.05 (3.07 ^c)	5.58 (5.64 ^c)	-
Mixed		3.83 ^b	4.41 (4.51 ^c)	8.19 (8.30 ^c)	-

Table 3.1: Solution energies (eV)

^areference [4]^breference [5]^creference[6]^dreference[7]

*: For Fe, the three positions compressed, tensile and mixed are the same. This is the intrinsic SIA energy.

Element	Cr	Ti	Y
Compressed	0.05 ^a	-0.35	-0.72
Tensile	-0.07 ^a	0.13	0.50
Mixed	0.08 ^a	-1.23	-2.11

Table 3.2: Binding energies SIA-solute(eV)

^areference[5]

3.1.2 Interactions with vacancies

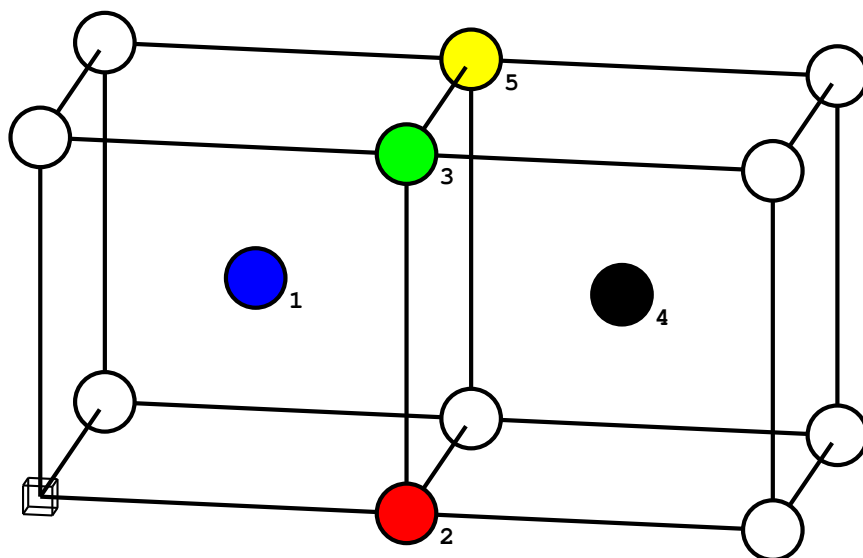
The interactions between the solutes and the vacancies are of prime importance. Indeed, the migration mechanism for the solutes occupying the substitutional positions is based on the vacancies according to the work of Le Claire [10] when their diffusion rate is of the same order of magnitude as the one of the host. In this study, this is at least the case for Cr and Ti, but it is less direct for Y. Moreover, a great quantity of vacancies are created during the irradiation process, hence determining their behaviour is necessary.

The first step is to determine precisely the geometry used. In most of the cases, the interaction will be negligible after a length corresponding to the diagonal of a primary BCC cell (as represented in Figure 3.2). In some rare cases, the calculations have been pursued further for reasons that will be explained. In Figure 3.2.a are represented the five nearest substitutional neighbours for a regular lattice position, and in figure 3.2.b the five nearest octahedral positions. Their distances are summed up in table 3.3.

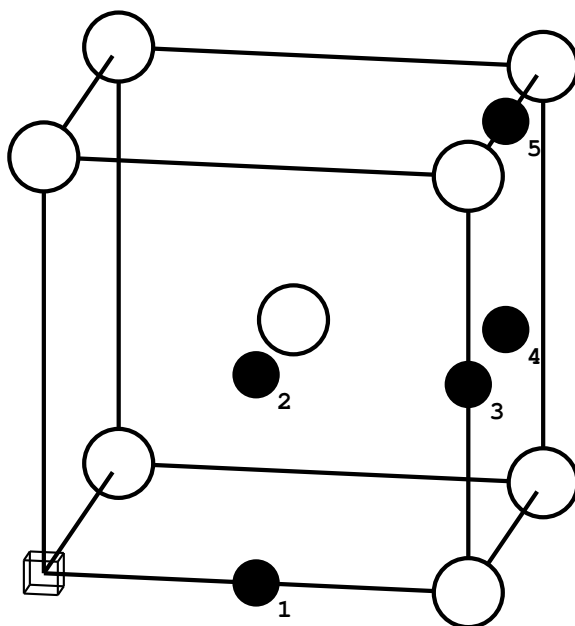
Nearest neighbour	1 st	2 nd	3 rd	4 th	5 th
Substitutional	0.87	1.00	1.41	1.58	1.73
Octahedral	0.50	0.70	1.12	1.22	1.5

Table 3.3: Distance between the nearest neighbours (in unit of lattice parameter)

Chromium and titanium have a negative solution energy in a substitutional lattice position, which means that they are even more stable than an iron atom in these sites. It is therefore a normal behaviour to be repulsive with a defect, if it directly tries to change the position of the substitutional atom, hence the repulsive attraction with a vacancy in first nearest neighbour. On the other hand, yttrium is much bigger than iron, and the vacancy



(a) substitutional



(b) octahedral

Figure 3.2: 5 nearest octahedral position from a regular lattice site

Element	Cr	Ti	Y	O
1NN	-0.24	0.24 ^b (0.26 ^a)	1.27 (1.45 ^a)	1.69 (1.65 ^a , 1.45 ^c)
2NN	0.00	-0.17 ^b (0.16 ^a)	0.20 (0.26 ^a)	0.73 (0.75 ^a , 0.60 ^c)
3NN	-0.01	0.01 ^b	0.13	0.14
4NN	-0.03	0.00 ^b	0.04	0.37
5NN	0.01	0.01 ^b	0.20	0.01

Table 3.4: Binding energies with a vacancy.

^areference[6]^breference[52]^creference[8]

offers it the possibility to relax from the lattice position and increase the distance with the surrounding iron atoms. As a consequence, they are strongly binding. This interaction will be studied with more details in section 3.1.3. The analysis of the strong attraction between oxygen and a vacancy will also be deepened.

In a more general view, the strength of the interaction decreases when the foreign atom and the vacancy get further away from each other. Since yttrium is so big, its range of effect is far-reaching and permits some considerations on the geometry. The interaction with the fifth nearest neighbour is indeed stronger than the one with the fourth. It can be explained by what is between the two defects in the crystal. In the case of the 5NN, there is only one atom, which can relax and allow the yttrium to relax in turn, whereas for the 4NN, the iron atoms corresponding to 1 and 2 on the picture 3.2.a will be on the way.

Chromium repels the vacancies in first nearest neighbour position. This will decrease the mobility of Cr atoms, since they are moving thanks to the vacancy diffusion mechanism. At longer distances, they are almost transparent to vacancies.

Titanium binds with the vacancy in first nearest neighbour, but repulses it in second nearest neighbour, while being transparent at longer distances. This results in both a difficulty for the vacancy to approach, and then to move away, which will also decrease the mobility. However, for both Cr and Ti, the binding energies are not that strong and will not prevent a displacement.

For yttrium on the other hand, the attractive energies in second and especially in first nearest neighbour with the vacancy are so strong that the vacancy is unlikely to move away. This drastically reduces the mobility of

Y atoms. It must also be added that the interaction between Y and a vacancy has a much longer range than for Cr and Ti which will have for effect to attract a vacancy jumping around from further, and therefore make the yttrium act as a vacancy trap.

The oxygen atoms are also strongly binding, but since both the vacancy and the oxygen can move without help of another species, it doesn't play a too big role on their mobility, although slowing both of them down. It allows a pair O-V to move together, one moving away and pulling the other, as illustrated in Picture 3.3. The vacancy and O start in position 1, then the vacancy is jumping to 2a, followed by the O in 2b and so on.

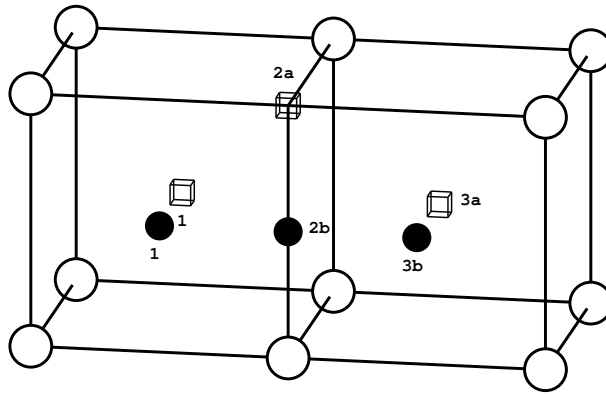


Figure 3.3: Illustration of a couple V-O moving.

3.1.2.1 The oxygen case

The strong binding between oxygens and vacancies, coupled to their high mobility suggests that they would find each other in a short time in the crystal. Once they form a pair, they lose some of their mobility, and assuming that the second oxygen would bind as strongly as the first one, the vacancy would be fixed in its position. It is then interesting to find out if a vacancy could be an oxygen sink.

From the table 3.5 can be seen that up to six oxygen atoms can be trapped in a vacancy. However, eight oxygens are highly unstable. For each number of oxygen atoms, all the configurations with the oxygens first and second nearest neighbours of the vacancy have been investigated and only the one with the highest binding energy has been displayed in picture 3.4. The relative binding energies have been calculated from the stable configuration with one less oxygen (or two, if the one with one less oxygen is not stable).

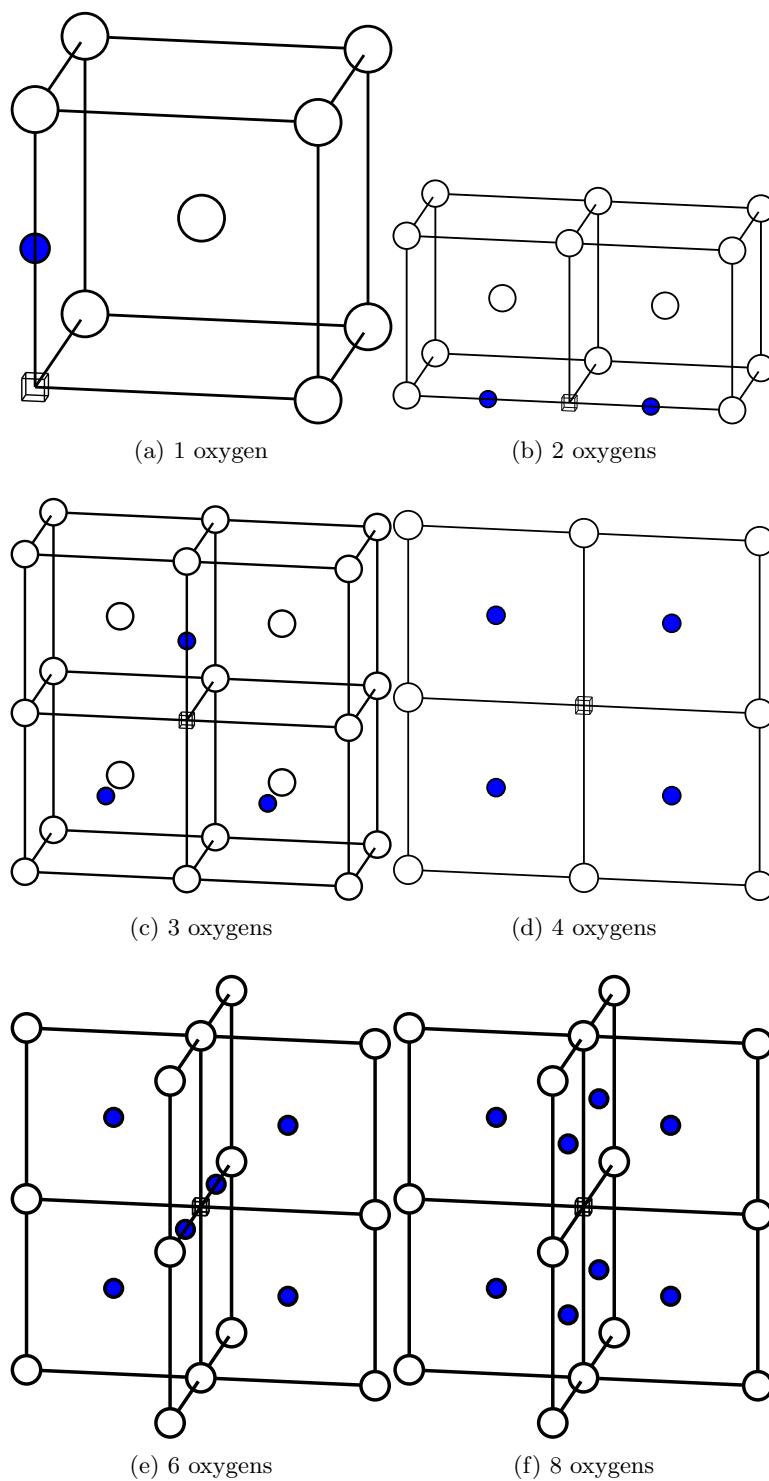


Figure 3.4: Geometry of vacancy-oxygen clusters.

Number of oxygen	Binding energy	Relative binding energy
1	1.69	-
2	3.50	1.81
3	3.83	0.33
4	4.01	0.18
6	5.88	1.87
8	-6.71	-12.59

Table 3.5: Binding and relative binding energies of oxygens with a vacancy.

For V-O₂, the two oxygens relax and form a dumbbell around the lattice position with no iron atom. The configuration with 3 O is the only one stable without being symmetric; no configuration with 5 O (not represented here) has been found stable either. Except for the V-O₅ system, all the systems for which the oxygen relaxation is toward the vacancy or negligible are binding, and the one with a relaxation in the opposite direction are repulsive (See picture 3.5). The V-O₃ system breaks a bit the trend, due to the non-symmetry.

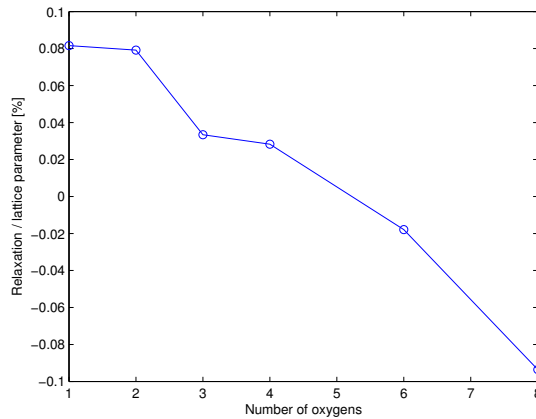


Figure 3.5: Relaxation of the oxygen atoms around a vacancy.

In the figure 3.6 are represented the differential charge densities of an iron matrix with one vacancy and one oxygen, and of an iron matrix with one vacancy and six oxygens. The differential charge density is defined as the difference between the charge density of the studied system and the charge density of each atom alone.

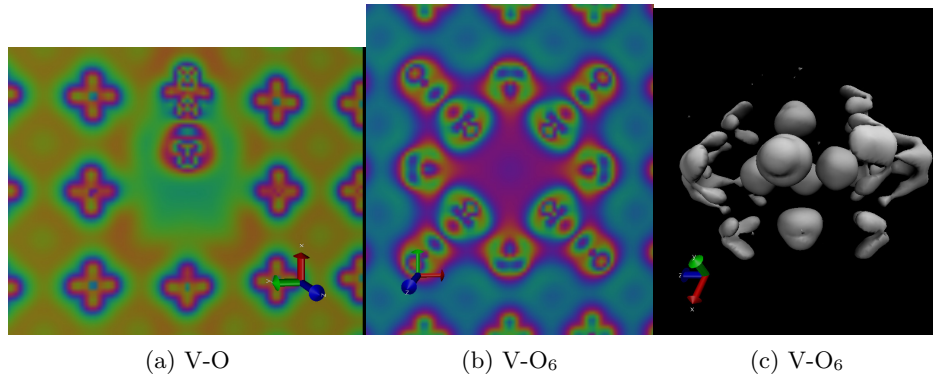


Figure 3.6: Differential electron density for 1 and 6 octahedral O around a vacancy.

The picture a. shows that O and V have a completely opposite charge, which suggest that they form an attractive ionic pair. Indeed, the binding energy between them is 1.69 eV. The picture b. proves that the charge is spatially confined around the vacancy. The charge cage present around a vacancy in an iron matrix [52] has not been strongly perturbed by the presence of oxygens (Fig c.). That can explain the binding character of this cluster.

3.1.3 Migration of the solutes

The migration energy of a solute in the iron host can be estimated by finding the Minimum Energy Path (MEP) thanks to a method such as the Nudged Elastic Band (NEB) one. This method is described in section 2.1.3.1. The diffusion mechanism considered for the solutes occupying the substitutional positions is the vacancy mechanism, and for oxygen, the jump between two octahedral positions, passing by a tetrahedral one.

The simulations have been done using 5 images in a supercell of 128 atoms with an energy cut-off of 450 eV and 27 K points. The results are displayed in table 3.6.

Element	Fe	Cr	Ti	Y	O
Migration energy	0.65	0.52	0.35	see section 3.1.3.1	0.48

Table 3.6: Migration energies of solutes in an iron BCC lattice.

The iron host has the highest barrier for the vacancy assisted migration,

0.13 eV higher than the Cr one and 0.30 eV higher than the Ti one. It means that they are more prone to jump when there is a vacancy in the first nearest neighbour position than Fe. Oxygen has around the same mobility as the solutes, but since they all can move without the help of a vacancy, and since they outnumber the vacancies by several orders of magnitude under normal conditions, they will finally move a lot more than the solutes. This is not true under irradiation, due to the creation of Frenkel pairs, described in section 2.3.3. It is worth noticing that these energies only depict the probability for an atom and a vacancy to exchange their positions, which is only a small part in the diffusion mechanism (see picture 3.9). Considerations made in section 3.1.2 about the vacancy attraction by a solute still apply.

3.1.3.1 The yttrium case

The yttrium case differs from the other ones due to the equilibrium position of this solute when it has a vacancy as first nearest neighbour. It indeed almost relaxes until the middle position, as shown in picture 3.7.a. The energy profile along the relaxation is plotted in picture 3.7.b. Due to the perfect symmetry of the crystal, the profile can be extended symmetrically to the other lattice position (originally the vacancy). The X-axis represents the displacement of the Y atom, 0 being the unrelaxed position, 100 being the vacancy initial position. The Y-axis is the energy of the system, relative to the energy of the system when the Y atom is not relaxed. Using the same migration definition as for the other solutes would obviously give a really small energy. It has been calculated to be 0.02 eV at 0 K, in accordance with the work of Murali [9]. At higher temperature, this barrier tends to be negligible, notably due to thermal oscillations. However, this energy seems in disagreement with the experimental work, which measure yttrium diffusing 400 times less fast than the iron at 1125 K [11].

As can be seen on the bar chart from picture 3.8, an ab initio molecular dynamic (MD) simulation for a time of more than 4 ps predict that the Y atom will stay between its initial position and the vacancy one. There is a high probability to find the Y in the middle at any given time. It can be noted that this MD simulation has been done at temperatures oscillating around 2000 K, and still, there is no jump, even though the material should be liquid. In the picture 3.8, 0 represents the unrelaxed Y position and 1 the unrelaxed V position.

However, in the vacancy diffusion mechanism, the vacancy is supposed to jump away from the solute before coming back. This mechanism is illustrated for the BCC lattice in the picture 3.9. The drawing b. shows the

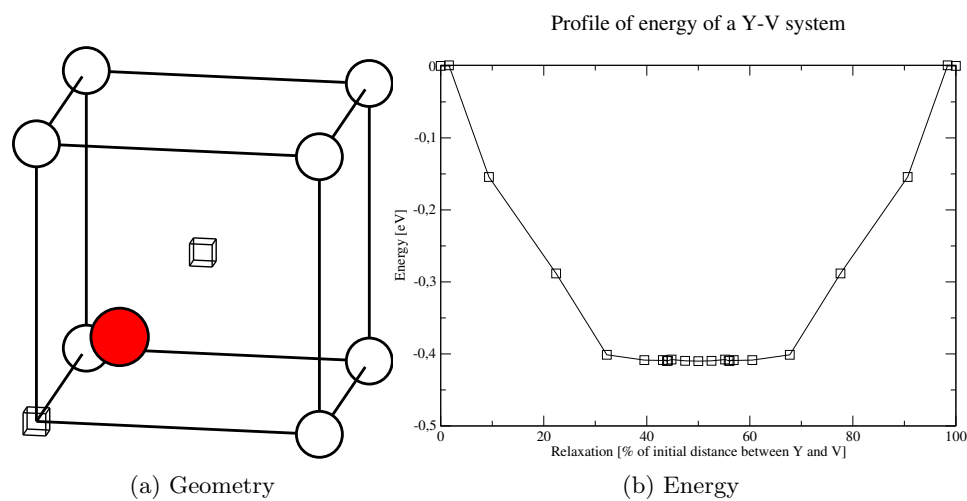


Figure 3.7: Illustration of the Y-V relaxation.

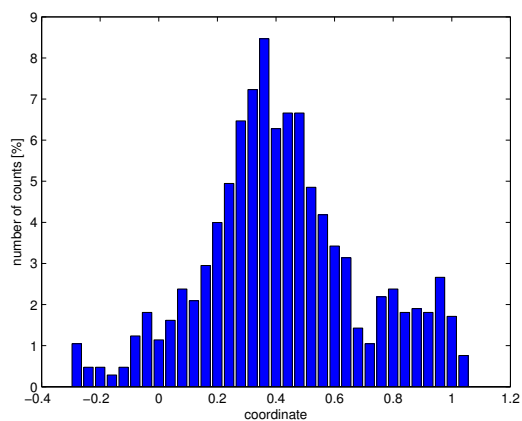


Figure 3.8: Position of the Y atom when first nearest neighbour of a vacancy for a temperature oscillating around 2000 K.

successive positions of the vacancy. However, when the yttrium has a vacancy in second nearest neighbour, it stays in a nearly non-relaxed position. It hence has to be given a sufficient energy to go back to the normal lattice position. That is this energy which dramatically slows down the diffusion of yttrium atoms. This energy is taken into account through the huge difference between the binding energies of an yttrium and a vacancy first and second nearest neighbour. It can be considered that the diffusion rate is contained in this binding energy, instead of in the migration energy for the other solutes.

However, this explanation is too simplistic. Indeed, if a Ti atom is added to the system in 2NN of the Y and 1NN of the vacancy, then the Y atom relaxes very little from the lattice position, and the migration energy becomes different from 0. The diffusion mechanism is then the classic one. It highly depends on the surroundings. It is nevertheless impossible to do ab-initio calculations for all the configurations existing, and implementing them in a tool to simulate the kinetics of the system would be extremely fastidious and inefficient. The computer power required would be much bigger for no significant changes in the results if the good approximations are made. Here, the natural approximation is to consider the diffusion mechanism governed by the vacancy attraction since around 90% of the atoms in the system are iron ones. That is the choice that has been made in his thesis work: to keep a low migration energy with a high vacancy attraction. It is further explained in section 3.2.1.

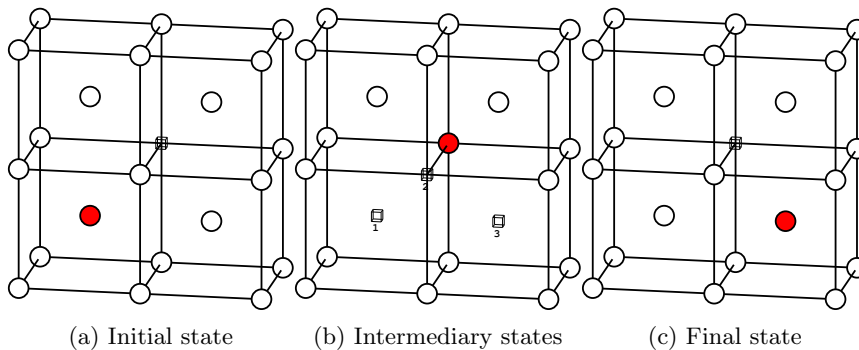


Figure 3.9: Illustration of the vacancy diffusion mechanism.

3.1.4 Interactions between solutes

Once the interactions between the solutes and the vacancies are characterized, it is important to determine the interactions among the solutes. They

will indeed be the force keeping the clusters together once they are formed thanks to the vacancies. Those are found using ab-initio simulations, with the same configuration and the same geometry as for the ones between the solutes and a vacancy.

Finally, since there is typically 9% or 14% of chromium in the steels to reduce the swelling and the DBTT, interactions between Cr and other solutes are calculated and results are displayed in table 7.

Element	Cr	Ti	Y	O
1NN	-0.27	-0.19	-0.18	0.10
2NN	-0.15	-0.22	-0.19	-0.06
3NN	-0.05	-0.12	-0.08	-0.20
4NN	-0.05	-0.02	-0.13	-0.14
5NN	-0.06	-0.07	-0.10	-0.09

Table 3.7: Binding energies of solutes with Cr.

The chromium is repulsive with everything, except with an oxygen in first nearest neighbour position. However, this attraction is small enough to not mean much at high temperatures. Since it has already been seen in the previous part that Cr and vacancies are repulsive, it is straightforward that Cr will not be part of a (Y,Ti,O) cluster. However, under 700 K and if the concentration is higher than 9%, Cr will strongly cluster. Since these data are calculated in the dilute limit, they fail to accurately describe the reality in this case. A more evolved potential is used in the part 3.2 to better describe the interactions between Fe and Cr and between Cr and Cr.

Then, the constituents of the wanted and experimentally observed clusters are studied and the results are displayed in the tables 3.7, 3.8, and 3.9. Ti repulses itself and repulses also Y, whereas Y can bind with itself. Without oxygen or vacancies, the only possible clusters are therefore yttrium ones, thanks to the second and third nearest neighbour binding interactions. However, oxygen can strongly bind with both Ti and Y and can therefore be the force which binds the three elements together. Vacancies are also produced in great quantities during irradiation and can then be the stabilizing power of the clusters.

3.1.4.1 The O-O case

O is stable in octahedral positions. It is then necessary to define the geometry used for the calculations. The idea is to keep the same range as

Element	Cr	Ti	Y	O
1NN	-0.19	-0.24 ^b (-0.29 ^a)	-0.29 (-0.28 ^a)	0.23 (0.27 ^a)
2NN	-0.22	-0.13 ^b (-0.15 ^a)	-0.19 (-0.15 ^a)	0.45 (0.55 ^a)
3NN	-0.12	-0.01 ^b	-0.08	-0.07
4NN	-0.03	-0.03 ^b	-0.02	-0.15
5NN	-0.07	0.01 ^b	-0.06	-0.13

Table 3.8: Binding energies of solutes with Ti.

^areference[6]^breference[52]

Element	Cr	Ti	Y	O
1NN	-0.18	-0.29 (-0.28 ^a)	-0.05 (-0.20 ^a)	-0.32 (-0.28 ^a)
2NN	-0.19	-0.19 (-0.15 ^a)	0.06 (0 ^a)	0.73 (0.85 ^a)
3NN	-0.08	-0.08	0.08	0.03
4NN	-0.13	-0.02	-0.04	-0.08
5NN	-0.10	-0.06	-0.11	-0.12

Table 3.9: Binding energies of solutes with Y.

^areference[6]

for the other solutes, which here brings us to the 11th nearest neighbour. An important point is that due to asymmetries, several distances have two corresponding positions.

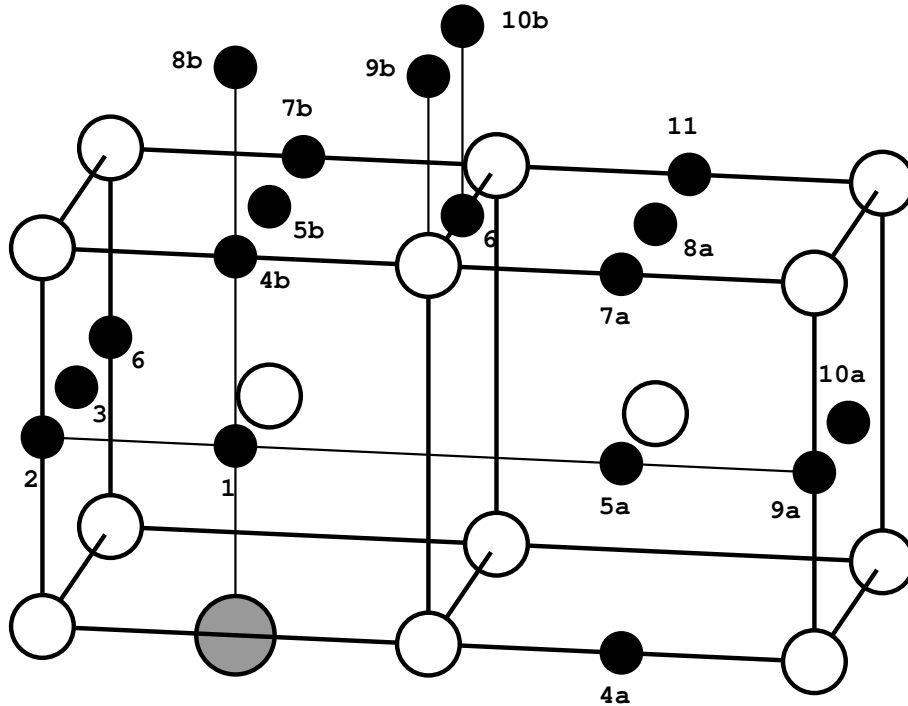


Figure 3.10: The eleventh nearest octahedral neighbours of an octahedral site.

The interaction between two oxygens is mostly repulsive and decreases with the distance. The configurations 4a and 10a are exceptions, due to the geometric configuration. The 4a state has 5 atoms on a line of 2 lattice parameters length and the 10a one has two normal lattice atoms between the two oxygens. This results in big stresses and so, the two O are strongly repulsive. The other exception is the configuration 4b which is attractive. This attraction is too weak to allow oxygen to cluster alone, but can maybe help determining the configuration of a cluster containing Y, Ti and O.

3.1.5 Clustering

As has already been discussed, clusters can not originate from a Y-Ti pair. On the other hand, it is quite obvious that any cluster with a vacancy will be stable. A more interesting consideration is whether or not the action of oxygen atoms is enough to keep the cluster whole, and which configuration

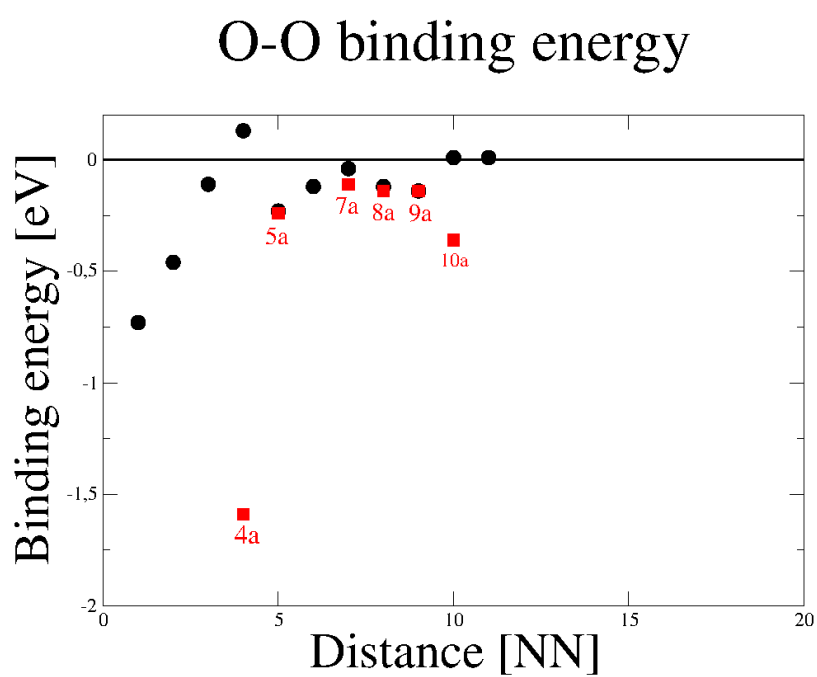


Figure 3.11: Binding energy of O with it's eleventh first nearest neighbours O.

would then be the most stable, i.e. have the lowest energy.

One has to be aware that this part is only based on pair interactions and could not be considered exact as a lot more atoms are considered. It is however a quick way to investigate billions of possible configurations and find the ones which are most likely to be strongly binding, before trying them out on VASP.

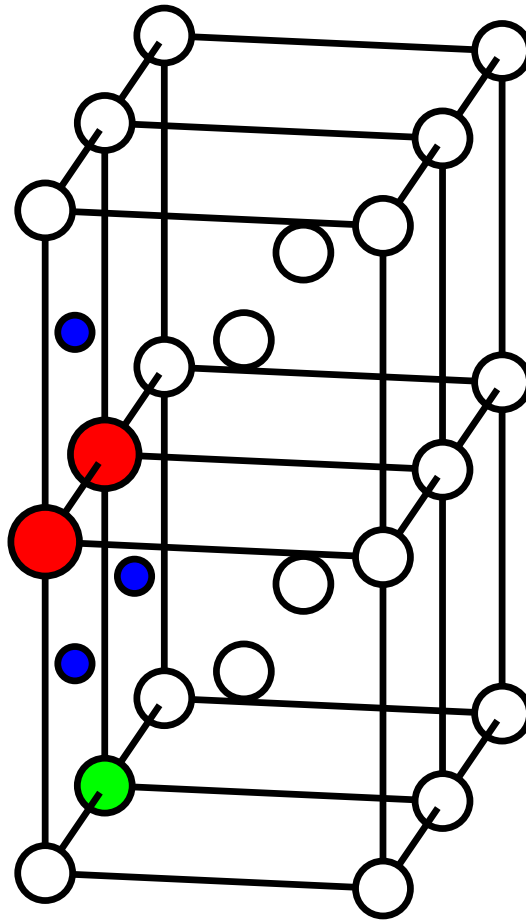


Figure 3.12: Most stable configurations for Y_2TiO_3 .

A program which tests all the possible configurations has been written and the results are displayed in figure 3.12. The blue atoms are oxygens, the red ones yttriums and the green ones titanium. The total binding energy for the geometry represented in a. is 4.34 eV, to compare with the one found by VASP which is 5.79 eV. It can also be compared to the 5.11 eV found by Jiang et Al. [6] for a different geometry of Y_2TiO_3 . This shows that it is in theory possible for Y_2TiO_3 to be stable without the help of a vacancy.

3.2 Atomic kinetic Monte-Carlo

The data from the ab initio calculations have been used in LAKIMOCA, an Atomistic Kinetic Monte Carlo code. This code is presented in section 2.2.2. Several modifications of the code have been made in order to simulate the systems of interest for this work. To keep the required calculating power reasonable, some approximations had to be done and are detailed in the next part.

3.2.1 Approximations and modifications

3.2.1.1 Changes in the code

The code has been originally written to handle solutes occupying substitutional positions. The treatment of the interstitial ones has been added thereafter and is a bit superficial. In order to have a better precision in the results, some portions of the code have been modified.

The first change was the oxygen-oxygen management. Previously, the code was handling them until the 4th nearest neighbour, without differentiating the 4a and 4b configurations (see figure 3.10), whereas calculations have shown that the binding energies for these two cases differ by 1.72 eV. It has been modified with the help of F. Nouchy [53] to take into account up to the 11th nearest neighbour with no significant loss in speed.

The second change was the second nearest interstitial neighbour management for the vacancy jumps. Previously, only the first one was taken into account, and first-principles results prove that handling the second one is important since Y-O and Ti-O are strongly binding in 2NN positions. It would have been possible to add the interactions until further than the 2NN, but the data presented in section 3.1.4 show that it is not useful for this work.

An essential change in the code that has not been made by lack of time is to handle the interactions between SIA and FIA. This is necessary if one want to simulate a steel under irradiation.

3.2.1.2 Approximations

In addition to these changes, some approximations have to be made here. Indeed, some parameters were causing too frequent jumps, having for consequence to reduce the length of the time-step too much and preventing from simulating more than a few microseconds. The main preoccupation while choosing the approximations was to keep an exact physics, changing only

the time dependence.

The migration energy of yttrium was so low that Y and V were exchanging positions in a infinitesimal time, preventing from observing the evolution or the formation of anything else. It has been set equal to the one of Ti, or 0.35 eV. In this way, it stays the lowest one in the system, but doesn't force the code to keep too small time steps.

In the same manner, the migration energy of oxygen, even if higher than the one of Ti, was still too low to enable clustering in a reasonable number of MC steps, since there is 300 oxygens in the considered systems. These 300 atoms correspond to 0.2% of oxygen in a MA957 steel (see table 2.2). It has been set to the carbon migration energy value, or 0.84 eV as opposed to the 0.48 eV found from the VASP simulaton.

3.2.1.3 Influence of interstitial atoms on the simulation time

The modifications of the migration energies of Y and O are not changing the physics but the conversion between the real time and the Monte Carlo time has to be adjusted to take it into account. Indeed, the Monte Carlo time is calculated from the migration probability by second defined in equation 2.19. The activation energy will change as the migration energy is changed, and in the exponential, it will yield a big difference.

In the same manner, the interstitial atoms jump independently from the vacancy and hence, the supersaturation coefficient (Eq 2.24) should not be applied to them. F. Nouchy proposed a solution, introducing a weight factor describing the nature of the jump (vacancy assisted, or interstitial) [53]. A different method has been developed here, using the supersaturation factor before adding up the jump probabilities of the vacancy and of the oxygens.

$$\Gamma_{tot} = \gamma \sum_{i=1}^8 \Gamma_i^V + \sum_{i=1}^N \sum_{i=1}^4 \Gamma_i^O \quad (3.1)$$

$$\gamma = \frac{C_V}{C_V^{eq}(T)}$$

Where γ is the inverse of the supersaturation factor, Γ represents the jump probability and V and O refer to vacancy and oxygen. A vacancy can exchange its position with its 8 first nearest neighbours and each oxygen atom (N in total) can jump to one of the 4 first nearest interstitial neighbour positions.

The equation 3.1 has to be compared to the one used in LAKIMOCA to find the time, which doesn't use the supersaturation coefficient. Since the

jump probabilities have been changed as well, one has to find a new factor to convert the MC time into the real time (C_{onv}).

$$C_{onv} = \frac{t_{MC}}{t_{real}} = \frac{\Gamma_{tot}^{mod}}{\Gamma_{MC}} = \frac{\gamma \sum_{i=1}^8 \Gamma_i^{V,mod} + \sum_{i=1}^N \sum_{i=1}^4 \Gamma_i^{O,mod}}{\sum_{i=1}^8 \Gamma_i^V + \sum_{i=1}^N \sum_{i=1}^4 \Gamma_i^O} \quad (3.2)$$

This equation can be simplified and expressed using the following variables.

$$X = \frac{\sum_{i=1}^N \sum_{i=1}^4 \Gamma_i^O}{\sum_{i=1}^8 \Gamma_i^V} \quad (3.3)$$

where N is the number of interstitial oxygens, Γ represents the jump probability.

$$Y = \frac{\sum_{i=1}^N \sum_{i=1}^4 \Gamma_i^{O,mod}}{\sum_{i=1}^N \sum_{i=1}^4 \Gamma_i^O} = \exp\left(\frac{\Delta E_{mig}}{k_B T}\right) \quad (3.4)$$

where N is the number of interstitial oxygens, Γ represents the jump probability and the mod exponent designates the probability with the new migration energy. ΔE_{mig} is the difference between the modified and the old migration energy values.

$$Z = \frac{\sum_{i=1}^8 \Gamma_i^{V,mod}}{\sum_{i=1}^8 \Gamma_i^V} = 1 - C + C \exp\left(\frac{\Delta E_{mig}}{k_B T}\right) \quad (3.5)$$

where Γ represents the jump probability and the mod exponent designates the probability with the new migration energy. ΔE_{mig} is the difference between the modified and the old migration energy values. C is the concentration of yttrium, or in a more general way, of solute whose migration energy has been modified. C is the ratio between the number of Y and the total number of atoms. C_0 has been defined the same way for oxygen.

Finally, C_{onv} can be expressed as

$$C_{onv} = \frac{\gamma Z + XY}{1 + X} \quad (3.6)$$

Ideally, this coefficient should be calculated at every step of the MC simulation. However, only a post simulation coefficient will be calculated in this study. One has to be aware that for this reason, and others such as vacancy trapping, abundantly discussed and illustrated by F. Nouchy [53], this coefficient gives only an idea of the real time, and could not be considered as more than a rough estimate.

γ can be calculated directly from the equation 2.25.

The other unknowns (X , Y and Z) has been calculated in average. For X , the assumptions are that the matrix is pure iron except for the considered defects. It means that both the vacancy and the O atoms are surrounded only by Fe atoms. It also means that X depends only on the temperature and on the number of oxygens.

In the same manner, Y and Z vary respectively with the temperature and the temperature and the yttrium concentration.

The results are displayed in table 3.10. It can be seen that the concentration of yttrium has no or little influence on C_{onv} . It can be explained by the fact that a vacancy assisted jump is already less probable than an oxygen jump, since there are so many more O atoms, whereas the concentration of V is orders of magnitude higher than the supersaturation limit. In addition to that, Y atoms represents only 0.2% of the total number of substitutional atoms. It also explains that the γ factor has a limited effect at these temperatures.

The main influence on C_{onv} is, as expected, due to the O. Their jumps are so likely that any change in their migration energy has a big effect.

Having a C_{onv} bigger than 1 means that the real time is slower than the MC time. It is the expected behaviour, since the mobility of several species in the matrix has been reduced artificially. However, without interstitial atoms, the supersaturation of vacancies is the predominant effect.

3.2.2 Formation of clusters

The goal here is to observe the formation of (Y,Ti,O) clusters in an iron matrix containing 9% Cr, 1% Ti, 0.2% Y and 300 O (0.2%). To observe which element has which effect, all of them has been added one by one and the resulting clustering has been studied. In the pictures displaying the results, neither Cr nor Fe are represented, as it would be impossible to observe anything relevant if they were. Ti atoms are in red, Y atoms in green, O atoms in blue and the vacancies in orange.

Firstly, since Y and Ti are believed not to cluster alone according to

T [K]	596	1200
γ	$5.02 \cdot 10^{-11}$	$3.06 \cdot 10^{-3}$
X	300 O: 5.48 500 O: 9.13	300 O: 28.98 500 O: 48.30
Y	911.17	29.51
Z	C=0.002: 2.01 C=0.005: 3.54	C=0.002: 1.04 C=0.005: 1.11
C_{onv}	C=0.002 and $C_0=0$: $1.01 \cdot 10^{-10}$ C=0.002 and $C_0=0.002$: 770.56 C=0.002 and $C_0=0.0033$: 821.22 C=0.005 and $C_0=0$: $1.78 \cdot 10^{-10}$ C=0.005 and $C_0=0.002$: 770.56 C=0.005 and $C_0=0.0033$: 821.22	C=0.002 and $C_0=0$: $3.18 \cdot 10^{-3}$ C=0.002 and $C_0=0.002$: 28.53 C=0.002 and $C_0=0.0033$: 28.91 C=0.002 and $C_0=0$: $3.40 \cdot 10^{-3}$ C=0.005 and $C_0=0.002$: 28.53 C=0.005 and $C_0=0.0033$: 28.91

Table 3.10: Value of the time conversion coefficient.

the pair interaction found in the ab initio study, iron matrix with (Cr,Ti), (Cr,Y) and (Cr,Y,Ti) are simulated. The results are shown respectively in picture 3.13, 3.14 and 3.15. For these three systems, no clustering is observed. It can just be noticed that when there is yttrium in the matrix, the chances that it traps the vacancy are high, due to the strong interaction Y-V in first nearest neighbour. This would result in a long time-step. From these simulations can be deduced that a ultra high density of nanoclusters can not be created without oxygen atoms or a vacancy to stabilize them.

The action of O is then investigated. As calculated in the section 3.2.1.3, the addition of oxygen atoms in the matrix will cause the time conversion coefficient to change dramatically. It is then nearly impossible to simulate long time-scales. However, at 1200 K, the migration of the solutes is fast, and the early nucleation stage can still be observed in a few μs . Again, to see the action of each element, different systems has been simulated. (Cr,Ti,O), (Cr,Y,O) and (Cr,Ti,Y,O) in an iron matrix has been studied and the results are presented in the pictures 3.16, 3.17 and 3.18.

The simulation including Cr, Ti, Y, and O proves that the clustering will occur in really short time-scales. Actually, even without titanium, a beginning of nucleation is observed, confirming the results of C. Hin et Al. [11] and extending them to the cases with Cr and Y. The (Cr,Ti,O) system has not be found to cluster. However, the time-scale is really short (37 μs for the real time), and the clusters might appear later. It would nevertheless be surprising since there is absolutely no beginning of ordering in time-scales

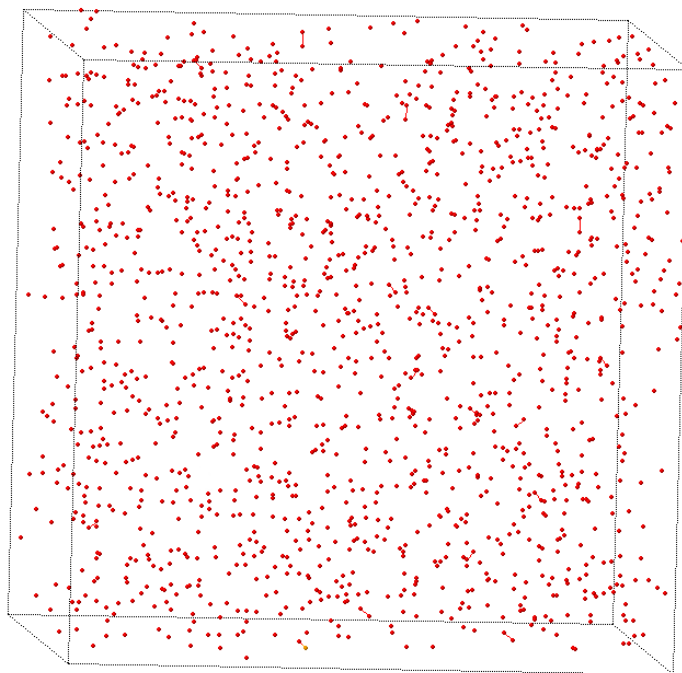


Figure 3.13: System Cr-Ti at 1200 K after 2.9 seconds.

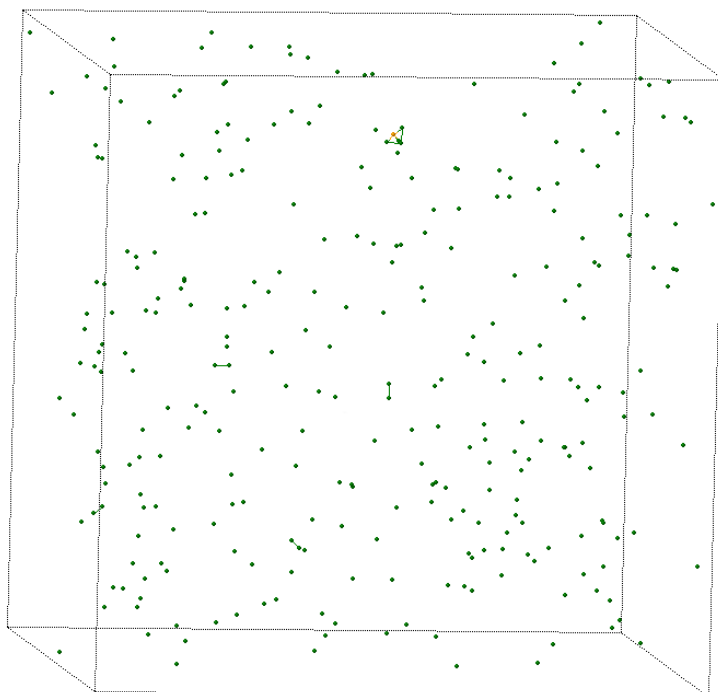


Figure 3.14: System Cr-Y at 1200 K after 98 days.

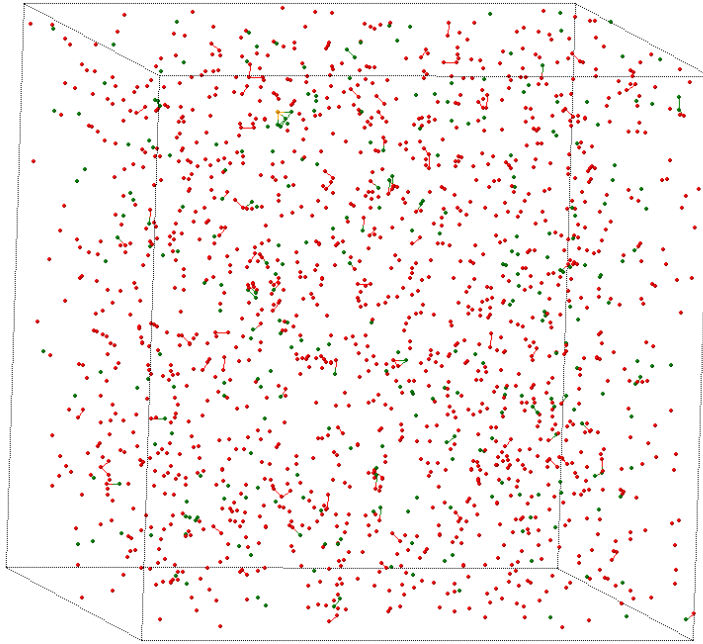


Figure 3.15: System Cr-Ti-Y at 1200 K after 90 days.

that permits a small clustering for the other systems. It can also be noted that there is a small cluster around the vacancy, suggesting that with a higher number of vacancies, under irradiation for instance, (Cr,Ti,O) could cluster.

A closer look is then given to the clusters in the (Cr,Ti,Y,O) system. Some of them are displayed in picture 3.19. However, this is still a really early nucleation stage, and they will change a lot while growing. A better analysis on the stoichiometry of these clusters should then be performed.

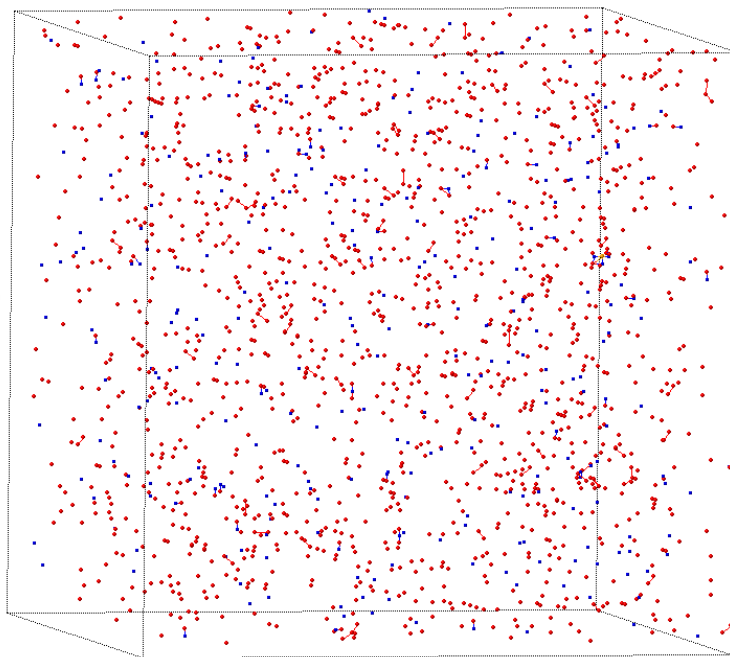


Figure 3.16: System Cr-Ti-O at 1200 K after 37 μs .

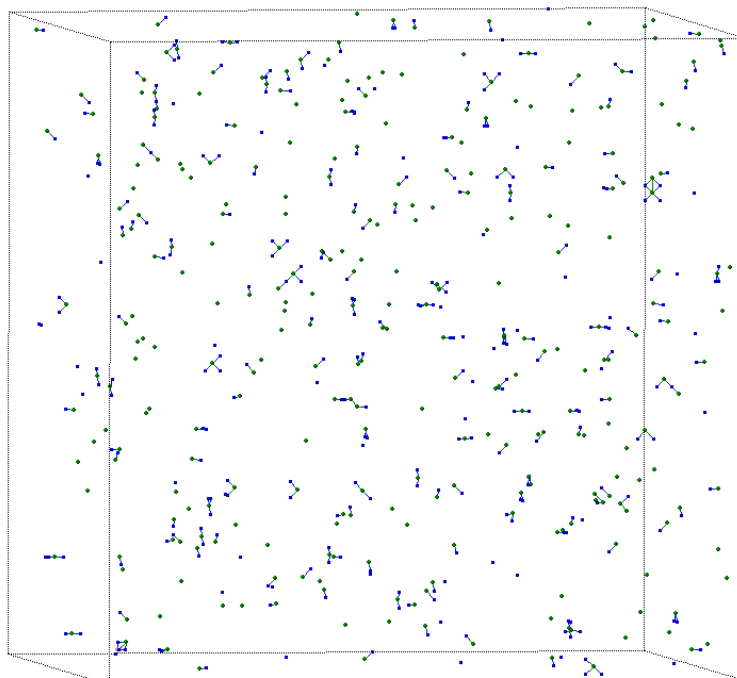


Figure 3.17: System Cr-Y-O at 1200 K after 127 μs .

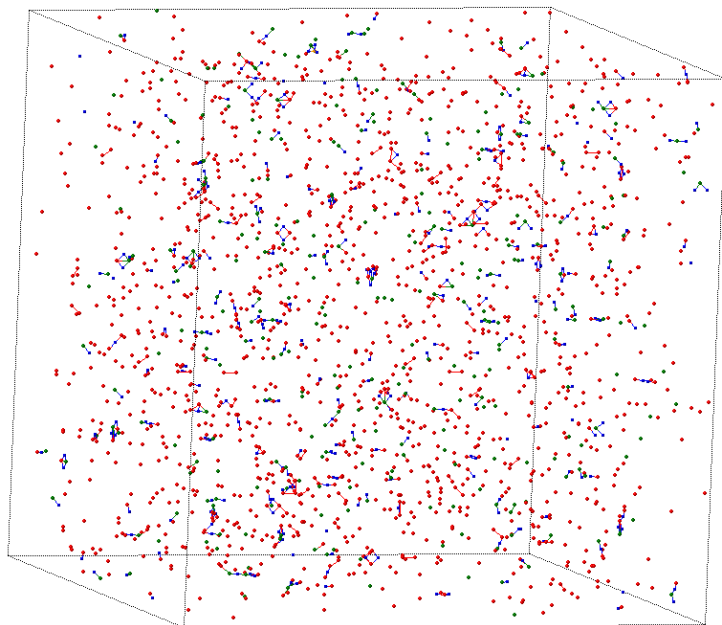
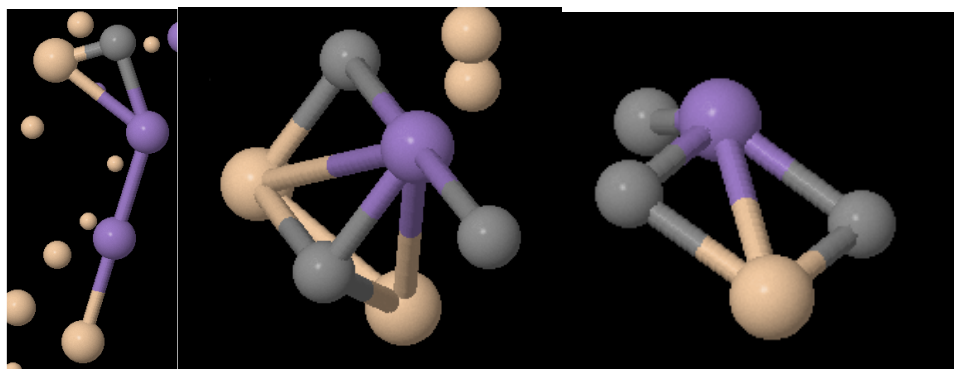


Figure 3.18: System Cr-Ti-Y-O at 1200 K after 153 μ s.



(a) Example of cluster Y_2Ti_2O (b) Example of cluster YTi_2O_3 (c) Example of cluster $YTiO_3$

Figure 3.19: Clusters at 1200 K after 153 μ s.

3.2.3 Stability of clusters under normal conditions

In this part, the temperature has been set at 596 K. To test the stability of the nanoclusters, several simulations have been made. Firstly, a Y_2TiO_3 cluster as found in the section 3.1.5, has been simulated alone with a vacancy, then several of these clusters far apart in the simulation box, and finally a much bigger cluster.

The new C_{ov} coefficients for (2Y,3O) and (10Y,15O) has been calculated using the formulas of the section 3.2.1.3 and are respectively 47.32 and 195.89 at 596 K.

For the simulation with just one cluster and one vacancy, it shows that the vacancy finds the cluster and makes it more stable. After more than 12 minutes (real time), the cluster is still complete and shows no announcing sign of splitting.

The test on 5 clusters is even more conclusive. Even if the real time is only around 2 seconds, the stability of the clusters has been observed without a vacancy to stabilize the other four. One oxygen sometimes jump from one cluster to another in a really short time. It is reasonable to assume that this stability will last for much longer, but a new simulation is necessary to prove it. However, due to the 15 oxygens in the system, the time conversion coefficient is unfavorable and data for 60 years would be extremely long and fastidious to acquire.

The same kind of behaviour is observed for the bigger cluster (5 times the size of a Y_2TiO_3 cluster), also for around two seconds. The vacancy finds the cluster and makes it more stable. Then an oxygen atom escape, but it probably comes from the fact that this cluster is not in the optimal geometric configuration.

Chapter 4

Conclusions

This work is composed of two main parts. In the first one, the goal was to find the binding energies of different defects in an iron lattice. This has been done thanks to the DFT framework, using the Vienna Ab-initio Simulation Package (VASP). In the second part, an atomistic kinetic Monte-Carlo code has been used to help interpreting the results, and visualize the dynamics of these defects.

In the part using first principles simulations, many basic geometric configurations with chromium, titanium, yttrium and oxygen have been investigated and characterized as binding or repulsive. These results are valid at 0 K and within the limits of the approximations, which were the size of the supercell, the sampling of the K points, the energy cut-off, the dilute limit, and the approximations inherent in the DFT, for both the Hamiltonian and the potential.

It has been shown that the chromium is not binding strongly with any other considered defects (vacancy, Ti, Y, O). Concerning titanium, it is respectively attractive and repulsive with a vacancy in first and in second nearest neighbour. It also repels Cr and Ti but attracts O at short ranges. Yttrium is bigger than the other atoms considered and will therefore bind very strongly with a close vacancy. The special case with Y and a vacancy in first nearest neighbour has been further investigated and the low diffusion coefficient has been explained. An oxygen atom binds also really strongly a vacancy at short ranges. It has been shown that a vacancy can actually bind up to 6 oxygens. They also bind with titanium in 1NN and 2NN positions, and with yttrium in 2NN position, whereas the 1NN one is strongly repulsive. The interactions between two oxygens in octahedral positions have been extensively studied, and it results from the calculations that two oxygens are significantly binding only when they are one lattice parameter away and

without an iron atom between them.

From these raw data, the theoretical possibility of forming (Y,Ti,O) clusters in the iron lattice have been discussed and proven. They can, according to the experiments, be Y_2TiO_3 as well as Y_2TiO_5 and $Y_2Ti_2O_7$.

The migration barriers of the different solutes have also been calculated, and the very specific case of the yttrium has been discussed. It has been concluded that the migration of an yttrium atom doesn't depend on its migration energy, but on the difference in binding with a vacancy in first and second nearest neighbour.

Possible improvements of this part of the work could be to consider always bigger supercells, with more K points and a higher energy cut-off. A preliminary part of this study has nevertheless been based on finding optimal parameters, combining reasonably converged results and fast calculations. It could also be useful to continue the database on binding energies for n-tuples instead of just for pairs. The influence of elements that are always in the steel but in lower quantity, such as Ni, Mo or W, could also be investigated.

In the second part, these results have been used in an Atomistic Kinetic Monte Carlo code (LAKIMOCA) to study the formation and the stability of these clusters. The migration energies of Y and O have been increased so they wouldn't keep the time-step too small. The influence of this change on the simulation time and on the real time has been quantified. This quantification has only been applied after the simulations. For better results, it is necessary to implement it into the code and to correct the time at each step.

LAKIMOCA has also been vastly modified to improve the treatment of the interstitial atoms. The temporal performances have not been deteriorated by more than 30 % after these changes.

The simulations have shown that clustering occur in the system thanks to the oxygen effect. Indeed, Y and Ti can apparently not cluster by their own. The chosen method has some major drawbacks: it considers that the attraction between two defects in an otherwise perfect iron lattice stays the same when the surrounding matrix is different. This has been briefly proven wrong by adding a titanium atom close to a Y-V pair during the study of the migration of yttrium. One other main issue is that this method doesn't allow a local change in lattice parameter or in crystal structure. When the clusters are big enough, they should impose the crystallographic properties locally. That is the reason why only the nucleation stage of the clusters can be studied with an AKMC code. The limit of the nucleation stage is hard to set, but the order of magnitude is a few tens of atoms.

The formation of nanoclusters at 1200 K has been proven, but only the

very early nucleation stage has been observed and the stoichiometry has hence not been determined. The stability of these clusters at 596 K has also been studied. Three different configurations have been investigated: one Y_2TiO_3 cluster with a vacancy, 5 Y_2TiO_3 far apart with a vacancy, and a bigger cluster of 30 atoms with the stoichiometry of Y_2TiO_3 and a vacancy. All of them tend to prove that the clusters are stable for a significantly long time.

The next step in this work is to study the stability of these clusters under irradiation. However planned at first, this has not been done by lack of time. It will necessitate further heavy modifications of LAKIMOCA to improve the way the SIA are treated. The other major improvement of this study would be to find a better way to handle the very likely events, so that they don't kill the simulations anymore by reducing the time-step too much. It has been shown that the main problem in that matter is caused by interstitial atoms, especially when their migration energy is low. This would permit to have longer simulations, so presumably bigger clusters, and then to study their stoichiometry and their size evolution.

Bibliography

- [1] M. Klimiankou, R. Lindau, and A. Möslang. Energy-filtered TEM imaging and EELS study of ODS particles and Argon-filled cavities in ferritic-martensitic steels. *Micron*, 2005.
- [2] S. Ukai, M. Harada, H. Okada, M. Inoue, and S. Nomura et al. Alloying design of oxide dispersion strengthened ferritic steel for long life FBRs core materials. *J. Nucl. Mater.*, 204:74–80, 1993.
- [3] S. Yamashita, S. Ohtsuka, N. Akasaka, S. Ukai, and S. Ohnuki. Formation of nanoscale complex oxide particles in mechanically alloyed ferritic steel. *Philos. Mag. Lett.*, 84:525–529, 2004.
- [4] Chu-Chun Fu and F. Willaime. Stability and Mobility of Mono- and Di-Interstitials in α -Fe. *Physical Review Letters*, 92,17:175503, 2004.
- [5] P. Olsson, C. Domain, and J. Wallenius. Ab initio study of Cr interactions with point defects in bcc Fe. *Physical Review B*, 75:014110, 2007.
- [6] Yong Jiang, John R. Smith, and G.R. Odette. Formation of Y-Ti-O nanoclusters in nanostructured ferritic alloys: A first-principles study. *Physical Review B*, 79:064103, 2009.
- [7] D. Murali, B.K. Panigrahi, M.C. Valsakumar, Sharat Chandra, C.S. Sundar, and Baldev Raj. The role of minor alloying elements on the stability and dispersion of yttria nanoclusters in nanostructured ferritic alloys: An ab initio study. *Journal of Nuclear Materials*, 403:113–116, 2010.
- [8] C.L. Fu, Maja Krčmar, G.S. Painter, and Xing-Qiu Chen. Vacancy Mechanism of High Oxygen Solubility and Nucleation of Stable Oxygen-Enriched Clusters in Fe. *Physical Review Letters*, 99:225502, 2007.

-
- [9] D. Murali, B.K. Panigrahi, M.C. Valsakumar, and C.S. Sundar. Diffusion of Y and Ti/Zr in bcc iron: A first principles study. *Journal of Nuclear Materials*, 419:208–212, 2011.
- [10] A.D. Le CLaire. *Physical Chemistry: An Advanced Treatise*, volume 10. Academic Press, New York, 1970.
- [11] C. Hin, B.D. Wirth, and J.B. Neaton. Formation of Y_2O_3 nanoclusters in nanostructured ferritic alloys during isothermal and anisothermal heat treatment: A kinetic monte carlo study. *Physical Review B*, 80:134118, 2009.
- [12] C. Hin and B.D. Wirth. Formation of oxide nanoclusters in nanostructured ferritic alloys during anisothermal heat treatment: A kinetic monte carlo study. *Materials Science and Engineering A*, 528:2056–2061, 2011.
- [13] W. Kohn. Nobel Lecture: Electronic structure of matter - wave functions and density functionals.
- [14] M. Born and R. Oppenheimer. Zur Quantentheorie der Molekeln. *Annalen der Physik*, 389,20:457–484, 1927.
- [15] K. Burke. *The ABC of DFT*. Department of Chemistry, University of California, 2007.
- [16] P. Hohenberg and W. Kohn. Inhomogeneous Electron Gas. *Physical Review*, 136:864–871, 1964.
- [17] W. Kohn and L.J. Sham. Self-Consistent Equations Including Exchange and Correlation Effects. *Physical Review*, 1340:1133–1138, 1965.
- [18] N.M. Harrison. *An Introduction to Density Functional Theory*.
- [19] W. Koch and M.C. Holthausen. *A Chemist's Guide to Density Functional Theory*. Wiley-VCH Verlag GmbH, 2001.
- [20] John P. Perdew, Kieron Burke, and Matthias Ernzerhof. Generalized Gradient Approximation Made Simple. *Physical Review Letters*, 77,18:3865, 1996.
- [21] Peter E. Blöchl, Clemens J. Först, and Johannes Schimpl. Projector augmented wave method: ab initio molecular dynamics with full wave functions. *Bull. Mater. Sci.*, 26:33–41, 2003.

- [22] Peter E. Blöchl, Johannes Kästner, and Clemens J. Först. Electronic structure method: Augmented Waves, Pseudopotentials and the Projector Augmented Wave Method. *Handbook of Materials Modeling*, 1:93–119, 2005.
- [23] D. Vanderbilt. Soft self-consistent pseudopotentials in a generalized eigenvalue formalism. *Physical Review B*, 41:7892–7895, 1990.
- [24] M.L. McKee and M. Page. *Reviews in Computational Chemistry*, volume IV. VCH Publishers Inc., 1993.
- [25] C.J. Cerjan and W.H. Miller. On finding transition states. *J. Chem. Phys.*, 75:2800, 1981.
- [26] University of Texas. Nudged Elastic Band. <http://theory.cm.utexas.edu/vtsttools/neb/>.
- [27] Hannes Jónsson, Greg Mills, and Karsten W. Jacobsen. Nudged elastic band method for finding minimum energy paths of transitions.
- [28] George H. Vineyard. Frequency Factors and Isotope Effects in Solid State Rate Processes. *J. Phys. Chem. Solids*, 3:121–127, 1957.
- [29] P. Olsson. *Modelling of Formation and Evolution of Defects and Precipitates in Fe-Cr Alloys of Reactor Relevance*. PhD thesis, Uppsala Universitet, 2005.
- [30] M.S. Daw, S.M. Foiles, and M.I. Baskes. The embedded-atom method: a review of theory and application, 1992.
- [31] W.T. Read. *Dislocations in crystals*. McGraw-Hill, 1953.
- [32] University of Kiel. Grain boundaries. http://www.tf.uni-kiel.de/matwis/amat/def_en/kap_7/backbone/r7_1_1.html.
- [33] G.H. Kinchin and R.S. Pease. The Displacement of Atoms in Solids by Radiation. *Rep. Prod. Phys.*, 18, 1955.
- [34] M.J. Norgett, M.T. Robinson, and I.M. Torrens. A proposed method of calculating displacement dose rates. *Nucl. Eng. Des.*, 33:50–54, 1975.
- [35] G.R. Odette, M.J. Alinger, and B.D. Wirth. Recent Developments in Irradiation-Resistant Steels.
- [36] Janne Wallenius and Merja Pukari. Cladding materials and radiation damage.

- [37] Stainless Steel 316 - Alloy Composition. <http://www.espimetals.com/index.php/online-catalog/202-stainless-steel-316-alloy-composition>.
- [38] M.L. Hamilton, D.S. Gelles, R.J. Lobsinger, M.M. Paxton, and W.F. Brown. Fabrication Technology for ODS Alloy MA957, 2000.
- [39] R. Lindau and A. Möslang, M. Rieth, and M. Klimiankou et Al. Present development status of EUROFER and ODS-EUROFER for application in blanket concepts. *Fusion Engineering and Design*, 75-79:989–996, 2005.
- [40] A. Möslang. The development and characterization of EUROFER ferritic-martensitic steel: the fusion perspective. In *Nuclear Fission & Fusion Steels Conference*, 2009.
- [41] F.A. Garner and H.R. Brager. The influence of Mo, P, C, Ti, Zr, Cr and various trace elements on the neutron-induced swelling of aisi 316 stainless steel. *Journal of Nuclear Materials*, 155-157:833–837, 1988.
- [42] F.A. Garner, M.B. Toloczko, and B.H. Sencer. Comparison of swelling and irradiation creep behavior of fcc-austenitic and bcc-ferritic/martensitic alloys at high neutron exposure. *Journal of Nuclear Materials*, 276:123–142, 2000.
- [43] S.I. Porollo, Yu.V. Konobeev, and S.V. Shulepin. Analysis of the behavior of 0Kh16N15M3BR steel BN-600 fuel-element cladding at high burnup. *Atomic Energy*, 106-4:238–246, 2009.
- [44] R.L. Klueh and D.J. Alexander. Embrittlement of 9Cr-1MoVNb and 12Cr-1MoVW steels irradiated in HFIR. *Journal of Nuclear Materials*, 187:60–69, 1992.
- [45] K. Yagi and F. Abe. Long-term creep and rupture properties of heat resisting steels and alloys. *Acta Metallurgica Sinica*, 11,6:391–396, 1998.
- [46] Y.T. Chiu and C.K. Lin. Effects of Nb and W additions on high-temperature creep properties of ferritic stainless steels for solid oxide fuel cell interconnect. *Journal of Power Sources*, 198:149–157, 2012.
- [47] M.K. Miller, E.A. Kenik, K.F. Russell, L. Heatherly, D.T. Hoelzer, and P.J. Maziasz. Atom probe tomography of nanoscale particles in ODS ferritic alloys. *Materials Science and Engineering A*, 353:140–145, 2003.

- [48] H. Kishimoto, K. Yutani, R. Kasada, O. Hashitomi, and A. Kimura. Heavy-ion irradiation effects on the morphology of complex oxide particles in oxide dispersion strengthened ferritic steels. *Journal of Nuclear Materials*, 367-370:179–184, 2007.
- [49] K. Yutani, H. Kishimoto, R. Kasada, and A. Kimura. Evaluation of Helium effects on swelling behavior of oxide dispersion strengthened ferritic steels under ion irradiation. *Journal of Nuclear Materials*, 367-370:423–427, 2007.
- [50] S. Jitsukawa, A. Kimura, A. Kohyama, R.L. Klueh, A.A Tavassoli, B. van der Schaaf, G.R. Odette, J.W. Rensman, M. Victoria, and C. Petersen. Recent results of the reduced activation ferritic/martensitic steel development. *Journal of Nuclear Materials*, 329-333:39–46, 2004.
- [51] J.H. lee, R. Kasada, H.S. Cho, and A. Kimura. Irradiation-Induced Hardening and Embrittlement of High-Cr ODS Ferritic Steels. *Journal of ASTM international*, 6,8, 2008.
- [52] P. Olsson, T.P.C. Klaver, and C. Domain. Ab initio study of solute transition-metal interactions with point defects in bcc Fe. *Physical Review B*, 81:054102, 2010.
- [53] F. Nouchy. Monte Carlo Simulations for Thermal Ageing in Welding Steels. Master’s thesis, Kungliga Tekniska Högskolan, 2012.